

学位論文

タンパク質の酸化に依存した細胞内シグナル伝達の
解析

**(Analysis of intracellular signaling depending
on protein oxidation)**

森中 紹文

Index

| | |
|--|-------|
| 1. 序論 | ...5 |
| 2. Abbreviations | ...9 |
| 3. TRX mediates oxidation-dependent phosphorylation of CRMP2 and growth cone collapse | ...11 |
| 3.1. Abstract | ...12 |
| 3.2. Introduction | ...13 |
| 3.3. Results | ...15 |
| 3.3.1. Identification of CRMP2 as a candidate substrate for TRX | ...15 |
| 3.3.2. Crucial importance of TRX-CRMP2 interaction in the Sema3A signaling | ...17 |
| 3.3.3. TRX reduces disulfide-linked CRMP2 homodimer induced by Sema3A | ...19 |
| 3.3.4. Sema3A stimulates H ₂ O ₂ generation via MICAL | ...21 |
| 3.3.5. TRX mediates oxidation-dependent CRMP2 phosphorylation | ...22 |
| 3.3.6. The molecular mechanisms of TRX-mediated CRMP2 phosphorylation | ...23 |
| 3.4. Discussion | ...25 |
| 3.5. Figures | ...28 |

| | |
|---|-------|
| 4. Oligomeric peroxiredoxin I is an essential intermediate for p53 to activate MST1 kinase and apoptosis | ...52 |
| 4.1. Abstract | ...53 |
| 4.2. Introduction | ...54 |
| 4.3. Results | ...56 |
| 4.3.1. Specific association of MST1 with oligomeric PRX I | ...56 |
| 4.3.2. PRX I mediates H ₂ O ₂ -induced MST1 activation | ...57 |
| 4.3.3. Cisplatin induces PRX I oligomer formation via p53 | ...59 |
| 4.3.4. PRX I mediates cisplatin-induced MST1 activation and cell death | ...60 |
| 4.3.5. Mechanism of MST1 activation by PRX I and H ₂ O ₂ | ...61 |
| 4.4. Discussion | ...64 |
| 4.5. Figures | ...67 |
| 5. Materials and Methods | ...87 |
| 5.1. Antibodies and reagents | ...87 |
| 5.2. Plasmid constructs and siRNA | ...88 |
| 5.3. Recombinant proteins | ...89 |
| 5.4. Cell culture and transfection | ...90 |
| 5.5. Non-reducing SDS-PAGE, native PAGE and immunoblotting | ...91 |
| 5.6. Identification of TRX target proteins | ...92 |
| 5.7. Preparation of rat DRG and growth cone collapse assays | ...92 |
| 5.8. Preparation of chicken DRG and growth cone turning assays | ...93 |
| 5.9. <i>In utero</i> electroporation and quantification of fluorescence intensities | ...94 |

| | | |
|--------------|---|--------|
| 5.10. | H ₂ O ₂ -imaging analyses | ...94 |
| 5.11. | <i>In vitro</i> kinase assay | ...95 |
| 5.12. | Apoptosis assay | ...95 |
| 5.13. | Real time PCR analyses | ...96 |
| 5.14. | Statistical analyses | ...96 |
| 6. | References | ...97 |
| 7. | Acknowledgement | ...109 |

1. 序論

過酸化水素 (H_2O_2) に代表される活性酸素 (reactive oxygen species: ROS) による酸化ストレスは、DNA の損傷やタンパク質の凝集を引き起こし、細胞を傷害する毒物としてよく知られている (1, 2)。近年、恒常的な酸化ストレスが、悪性腫瘍や糖尿病、そして神経変性疾患など様々な疾患の原因となっている可能性が指摘されており、活性酸素による細胞内シグナル伝達の分子メカニズムを解き明かすことの重要性が叫ばれている (1, 2)。

その一方で、活性酸素は細胞内において能動的に産生される生理的なセカンドメッセンジャーとしての側面を持つことが知られている (3-5)。実際に、上皮成長因子や腫瘍壊死因子によるシグナル伝達における活性酸素の働きなどはよく解析されており、特定のタンパク質を酸化し、その機能を制御することでシグナルを伝達していることが判っている (3-5)。例えば、上皮成長因子によるシグナル伝達では受容体のチロシンリン酸化の増加に活性酸素が重要な役割を果たしている。上皮成長因子がその受容体に結合すると、NADPH オキシダーゼが活性化され、活性酸素を産生する。産生された活性酸素はリン酸化チロシン脱リン酸化酵素を酸化することで不活性化し、受容体のチロシンリン酸化を増進させる。受容体はチロシンリン酸化によって活性化されるため、受容体はさらに活性化され、下流へのシグナル伝達が増幅されるのである。また、腫瘍壊死因子によるシグナル伝達ではその中心となるリン酸化酵素 ASK (apoptosis signal-regulating kinase) の活性化に活性酸素の産生が重要な役割を果たしている。上皮成長因子と同じく、腫瘍壊死因子がその受容体に結合すると、NADPH オキシダーゼが活性化され、活性酸素を産生する。産生された活性酸素は、ASK に結合して抑制するタンパク質チオレドキシンを酸化する。酸化されたチオレドキシンは ASK から乖離して抑制できなくなるため、ASK が活性化されてシグナルが下流へと伝

達される。

活性酸素がタンパク質の機能を制御する主要なメカニズムはシステイン残基の酸化である (3-5)。システイン残基はそのチオール基が酸化されると、スルフィニル基となったり、二つのチオール基の間でジスルフィド結合を形成する。これによってタンパク質の反応中心が影響を受けたり、立体構造が変化するため、その機能が調節されるのである。システイン残基のチオール基は反応性が非常に高く、酵素反応の活性中心として働くことが多い。酸化されるチオール基が酵素反応の活性中心であった場合、その酵素活性も影響を受け、大抵は失活する。この例としてはリン酸化チロシン脱リン酸化酵素やタンパク質分解酵素カスパーゼ、過酸化水素分解酵素ペルオキシレドキシシンなどがよく知られる (3-5)。ジスルフィド結合の形成によってタンパク質の構造が変化し、機能が調節される場合も多い。この例としては前述のチオレドキシシンやプロテインキナーゼ G などが挙げられる (3-5)。チオレドキシシンは分子内ジスルフィド結合を形成するとその構造が変化し、ASK と結合できなくなり、従って抑制もできなくなる。プロテインキナーゼ G は分子間ジスルフィド結合によるホモ二量体を形成すると、互いに自己リン酸化して活性化する。以上のように、活性酸素によるシグナル伝達の分子メカニズムは徐々に明らかにされつつある。しかし、その多くは未だ解明されておらず、どのようなタンパク質が活性酸素の「受容体」として酸化され、シグナルを下流へと伝達しているのかはほとんど判っていないのが現状である。私はこれを解明するため、「酸化されやすいタンパク質を網羅的に探索する」、「活性酸素に応答するとして既知のタンパク質が、シグナル伝達の中枢にあるタンパク質を制御している可能性を検討する」という二つのアプローチを採った。

細胞内シグナル伝達において、活性酸素はあらゆるタンパク質を酸化するのではなく、特定のタンパク質のみを標的として酸化している。当然、標的となるタンパク質は他のタンパク質と比較して、より酸化されやすいと考えられる。そこで、細胞内にお

いて酸化されやすいタンパク質を網羅的に探索し、その中にシグナル伝達の中心となるタンパク質があれば、そのタンパク質が活性酸素の「受容体」としてシグナル伝達を制御しているのではないかと考えられる。このアプローチにおける最大の問題点は、どのようにして酸化されるタンパク質を同定するのかである。そのための方法として、酸化されたシステイン残基をビオチンなどの低分子で標識し、その標識をアフィニティー精製することで酸化されたタンパク質を精製するという方法がある (6)。しかし、この方法では酸化されていないシステイン残基も標識されてしまうことが多く、非特異的に考えられるタンパク質が非常に多く精製されてしまうのが難点である。そこで私はこの問題点をジスルフィド結合還元酵素チオレドキシンを活用することで解決できるのではないかと考えた。チオレドキシンはジスルフィド結合を還元する、つまり酸化されたタンパク質を還元する酵素であるため、その基質は必然的に酸化されやすいタンパク質であると考えられる (7, 8)。そのため、チオレドキシンの基質を網羅的に探索することで、酸化されやすいタンパク質を同定できるのである。さらに、チオレドキシンには反応中間体として基質と結合したまま乖離できない変異体が知られており、この変異体を活用すればチオレドキシンの基質を網羅的に同定できる (9)。この方法は新たに工夫を施すことで、前述の方法よりも非特異的に同定されるタンパク質が少なく、より精度の高い分析が可能であった。このアプローチによる研究を、本論文にて " TRX mediates oxidation-dependent phosphorylation of CRMP2 and growth cone collapse " として報告する。

酸化されるタンパク質それ自身がシグナル伝達の中枢を担うタンパク質であれば前述のアプローチに問題はない。しかし、酸化されるタンパク質は別であり、そのタンパク質がシグナル伝達の中心にあるタンパク質を制御しているという可能性も多分にありえる。実際、シグナル伝達の根幹をなすタンパク質がちょうど酸化されやすく、しかも酸化されるとタンパク質の機能がうまく調節されるようなシステイン残基を持ってい

る可能性は高くないと考えられる。それよりも活性酸素の「受容体」として特化したタンパク質が存在し、そのタンパク質が活性酸素のセンサーとしてシグナル伝達の中心にあるタンパク質を調節していると考えの方が合目的的であると私は考えた。そこで、私は活性酸素に応答してその構造が変化するタンパク質として、最も有名なタンパク質の一つであるペルオキシレドキシシンに焦点を当て、ペルオキシレドキシシンがシグナル伝達における活性酸素の「受容体」として働いている可能性を検討した (10)。このアプローチによる研究を、本論文にて " Oligomeric peroxiredoxin I is an essential intermediate for p53 to activate MST1 kinase and apoptosis " として報告する。

2. Abbreviations

BCIP 5-bromo-4-chloro-3'-indolylphosphatase *p*-toluidine

BSA bovine serum albumin

CDK5 cyclin-dependent kinase 5

CRMP2 collapsin response mediator protein 2

DAPI 4',6-diamidino-2-phenylindole

DHC dynein heavy chain

DMEM Dulbecco's modified Eagle medium

DNCB 2,4-dinitro-1-chlorobenzene

DRG dorsal root ganglion

DTT dithiothreitol

FBS fetal bovine serum

GSK3 glycogen synthase kinase 3

IAA iodoacetamide

JNK c-Jun N-terminal kinase

KLC kinesin light chain 1

MEF murine embryonic fibroblast

MICAL molecule interacting with CasL

MST mammalian Ste20-like kinase

NAC N-acetyl cysteine

| | |
|--------|-------------------------------------|
| NBT | nitro-blue tetrazolium chloride |
| NGF | nerve growth factor |
| NP-1 | neuropilin-1 |
| NRX | nucleoredoxin |
| PAGE | poly-acrylamide gel electrophoresis |
| PBS | phosphate buffered saline |
| PEITC | β -phenylethyl isothiocyanate |
| PlexA | plexin-A |
| PRX | peroxiredoxin |
| ROS | reactive oxygen species |
| SDS | sodium dodecyl sulfate |
| Sema3A | semaphorin 3A |
| TRP14 | thioredoxin related protein 14-kDa |
| TRP32 | thioredoxin related protein 32-kDa |
| TRX | thioredoxin |
| TxR | thioredoxin reductase |

3.

**TRX mediates oxidation-dependent phosphorylation
of CRMP2 and growth cone collapse**

3.1. Abstract

Sema3A is a repulsive guidance molecule for axons by inducing growth cone collapse through phosphorylation of CRMP2. However, its mechanistic details remained unknown. I here show a quite unexpected role of CRMP2 oxidation and TRX in regulation of CRMP2 phosphorylation and growth cone collapse. Sema3A stimulation generates H₂O₂ via MICAL and oxidizes CRMP2 to form a disulfide-linked homodimer through Cys504. Oxidized CRMP2 then forms a transient disulfide-linked complex with TRX, which stimulates phosphorylation by GSK3 and growth cone collapse. Moreover, I succeeded in reconstituting oxidation-dependent phosphorylation of CRMP2 *in vitro*, using a limited set of purified proteins. my results not only clarify the importance of H₂O₂ and CRMP2 oxidation in Sema3A-induced growth cone collapse, but also indicate an unappreciated mechanism of TRX action, which links CRMP2 oxidation to phosphorylation.

3.2. Introduction

Various axon guidance molecules underlie the proper development of the highly ordered nervous system, which steer axons by regulating cytoskeletal dynamics in growth cones (11-14). Sema3A is a repulsive guidance molecule that induces growth cone collapse to repel axons (Figure 1A) (12-14). Sema3A binds and activates the receptor NP-1 and PlexA to regulate the cytoskeleton through CRMP2 (15-17). CRMP2 associates with tubulin heterodimers and promotes microtubule polymerization (18). Upon Sema3A stimulation, CDK5 phosphorylates CRMP2 at Ser522, which acts as a priming site for GSK3-dependent phosphorylation, and subsequently GSK3 phosphorylates at Thr509, Thr514, and Ser518 of CRMP2 (16, 17, 19). These phosphorylations lead to microtubule disassembly and following growth cone collapse. Thus, the regulatory mechanism of CRMP2 phosphorylation has been regarded as a central subject for Sema3A signaling, but its precise molecular mechanism remains largely obscure.

In addition to CRMP2, MICAL has emerged as an essential mediator of Sema-dependent axon guidance (20, 21). MICAL possesses a flavoprotein monooxygenase domain and requires this domain to steer axons, suggesting the possibility that redox signaling plays a crucial role in Sema3A signaling. Indeed, it is reported that mammalian MICAL can generate H₂O₂ (21, 22), a representative of ROS, and that a flavin monooxygenase inhibitor (-)-epigallocatechin gallate blocks Sema3A-induced axonal repulsion (20, 23). However, there has been no definitive evidence that MICAL actually produces H₂O₂ upon Sema3A stimulation *in vivo*. Very recently, it was reported that *Drosophila* MICAL directly regulates actin reorganization

through the flavoprotein monooxygenase domain (24). However, it still remains unknown whether it occurs via H₂O₂ generation and whether there is any functional relationship between MICAL and CRMP2.

Excess ROS cause oxidative stress and ultimately activate signaling pathways leading to cell death, whereas moderate amount of ROS can mediate various physiological phenomena such as cell proliferation and motility (2-5). Especially, there has been accumulating evidence that H₂O₂ can function as a second messenger by oxidizing cysteine residues to form disulfide bonds in various target proteins and regulate their function (Figure 1B). Intracellularly formed disulfide bonds are normally reduced to thiols mainly by TRX, a thiol-oxidoreductase conserved in both prokaryotes and eukaryotes (7-9). TRX reduces disulfide bonds through thiol-disulfide exchange between the target proteins and its CXXC active site residues. Considering that H₂O₂ mediates signal transduction through cysteine oxidation, it is highly likely that proteins involved in ROS signaling are substrates of TRX. Therefore, the identification of TRX substrates is expected to give me an important clue to discover a novel key player in ROS signaling.

Here I performed an *in vivo* screening for candidate TRX substrates by a substrate-trapping method and identified CRMP2. CRMP2 was oxidized to form a disulfide-linked homodimer via Cys504 by Sema3A stimulation, which was dependent on the generation of H₂O₂ by MICAL. Unexpectedly, CRMP2 oxidation promoted the disulfide-linked interaction with TRX and GSK3-dependent phosphorylation, resulting in growth cone collapse.

3.3. Results

3.3.1. Identification of CRMP2 as a candidate substrate for TRX

Two cysteine residues (Cys32 and 35) conserved in TRX are directly involved in the oxidoreductase reaction (7, 8, 25). The C35S mutant form of TRX has been utilized in substrate-trap experiments, because it can form mixed disulfide-linked complexes with TRX substrate proteins (9), and by reduction with DTT these complexes can be released (Figure 2A). To search for TRX substrate proteins under physiological conditions, I generated NIH-3T3 cell lines stably expressing FLAG-TRX C35S and FLAG-TRX C32/35S (negative control). Cell lysates were immunoprecipitated with anti-FLAG antibodies and candidate proteins were eluted with DTT. Obtained samples were resolved by SDS-PAGE and visualized by silver staining (Figure 2B). Mass spectrometry revealed that an abundant protein in the 65-kDa region is CRMP2. Using the same method, I also identified several well-characterized TRX substrates, such as peroxiredoxin I and II (10), supporting the validity of this experimental system. Previously, CRMP2 was identified as a necessary mediator of Sema3A-induced growth cone collapse (15) and also plays an important role in establishing the neuronal polarity (19, 26).

To confirm the interaction between TRX and CRMP2, I performed co-expression and co-immunoprecipitation analyses. As shown in Figure 3A, Myc-CRMP2 bound to FLAG-TRX C35S but not to FLAG-TRX wild type (WT) or C32/35S, indicating the requirement of Cys32, which is known to be the redox-active cysteine residue in TRX. Next, I treated the lysates with IAA to block further oxidation of cysteine residues and prevent non-specific interaction between thiols after harvesting cells *in vitro*. The

IAA-treated lysates were then resolved by non-reducing SDS-PAGE. The results clearly showed a 75-kDa signal that matches well with the molecular mass of the TRX-CRMP2 disulfide complex (Figure 3B). When cells were treated with H₂O₂ to induce disulfide bonds, TRX WT also formed a disulfide complex with CRMP2. Proteins with a TRX-related sequence containing the catalytic cysteine residues constitute a large family (7, 8, 25), including NRX (27), TRP32 (28), and TRP14 (29), which exist in the cytoplasm. To investigate the specificity of the interaction, I generated mutants of these TRX family proteins corresponding to TRX C35S and tested their binding ability to CRMP2. Only FLAG-TRX C35S associated with Myc-CRMP2 (Figure 4A), indicating that the interaction is specific to TRX among the TRX family proteins examined. Next I examined whether endogenous TRX interacts with CRMP2 by immunoprecipitation assays using anti-CRMP2 antibodies and N1E-115 neuroblastoma cell lysates both treated with H₂O₂ and untreated. Cell lysates were treated with IAA as described above and subsequently precipitated with acetone to make proteins denatured and dissociate non-covalent binding proteins (30). The results indicated a clear co-immunoprecipitation of TRX with CRMP2 when cells were treated with H₂O₂ (Figure 4B). As CRMP2 was predicted to interact with TRX Cys32 through a disulfide bond, I tried to identify which cysteine residues of CRMP2 were responsible for the interaction. The cysteine residues conserved between human and mouse were substituted for serine residues. Among these mutants, only Myc-CRMP2 C504S did not associate with FLAG-TRX C35S (Figure 5A), suggesting that Cys504 is crucial for the interaction with TRX. To further examine the cysteine-dependent interaction, I used recombinant proteins of TRX and CRMP2 to conduct GST pull-down assays. His-TRX C35S was specifically pulled down by CRMP2-GST, and the interaction was augmented

by oxidation (Figure 5B). Moreover, His-TRX C35S did not associate with CRMP2-GST C504S, irrespective of its redox state. Collectively, these results support the notion that TRX Cys32 is directly linked with CRMP2 Cys504 through a disulfide bond. A previous study indicated that S-nitrosylation occurs at CRMP2 Cys504, which also supports that Cys504 is a redox active cysteine residue (31, 32).

3.3.2. Crucial importance of TRX-CRMP2 interaction in the Sema3A signaling

CRMP2 is necessary for Sema3A-induced growth cone collapse of DRG neurons (15-17), and thus I next investigated the importance of TRX in Sema3A signaling. First, I examined whether endogenous TRX proteins exist in growth cones using immunofluorescence microscopy, and the results clearly confirmed their presence (Figure 6A). Next, I expressed Myc-CRMP2 C504S, which does not bind TRX, in neurons because CRMP2 is necessary for Sema3A-induced growth cone collapse (17), and confirmed the presence of expressed proteins in growth cones (Figure 6B). As shown in Figure 7A, Myc-CRMP2 C504S suppressed the extent of growth cone collapse, as did Myc-CRMP2 T509A/S522A, which was the phosphorylation-inactive mutant known to function in a dominant-negative manner and used as a positive control (the rationale for this dominant-negative effect by CRMP2 C504S is explained in Discussion). These results suggested the importance of Cys504, which is crucial for the interaction with TRX, in Sema3A signaling. To directly examine the importance of TRX in Sema3A signaling, the effect of FLAG-TRX overexpression was investigated. I used the TRX C32/35S mutant that is reported to compete for TxR and thus inhibits the function of endogenous TRX (33). As a result, growth cone collapse was repressed in DRG neurons expressing FLAG-TRX C32/35S compared with those expressing

FLAG-TRX WT (Figure 7B), suggesting the importance of TRX. In contrast, FLAG-TRX C35S that can bind CRMP2 showed no effect as WT. To further confirm these findings, I performed knockdown experiments using three different siRNAs against TRX. Western blot analyses indicated that the siRNAs partially suppressed the expression of TRX at different efficiencies (Figure 8A). The growth cone collapse assays revealed the importance of endogenous TRX in Sema3A-signaling. Moreover, I performed rescue experiments to exclude the possibility of the off-target effects using the TRX rescue (Rsc) mutant, which has three silent mutation in the target sequence and thus resistant to TRX siRNA. The results shown in Figure 8B clearly indicate that expression of FLAG-TRX Rsc restores normal collapse response. In addition, the inhibition rate appeared to reflect the knockdown efficiency of each respective siRNA. In contrast, there was no significant effect on serum-induced phosphorylation/dephosphorylation of various proteins (Figure 8C), implicating that TRX-knockdown rather specifically affect Sema3A-induced growth cone collapse.

To further establish the importance of TRX-CRMP2 interaction in Sema3A signaling, I examined the turning behavior of growth cones in response to Sema3A gradient. Directional application of Sema3A causes repulsive growth cone turning in culture (11-13, 34). As shown in Figure 9A, bath application of a TxR inhibitor DNCB, which forces TRX to take an inactive form via inhibition of TRX regeneration by TxR (35), suppressed Sema3A-induced repulsive turning of growth cones in DRG neurons. Moreover, the expression of Myc-CRMP2 C504S also showed inhibitory effect on growth cone repulsion, while Myc-CRMP2 WT had no significant effect (Figure 9B). Next, to confirm the *in vivo* importance of the TRX-CRMP2 interaction, I performed *in utero* electroporation analyses because Chen *et al.* reported that Sema3A signaling is

important for the radial migration of cortical neurons during development (36). Myc-CRMP2 WT or C504S-expressing plasmids were transfected into E14.5 mouse brains and the radial migration of cortical neurons was examined. As shown in Figure 10, A and B, Myc-CRMP2 C504S perturbed the migration of cortical neurons, while Myc-CRMP2 WT showed no significant effect. These migration defects resemble those seen in NP-1-conditional knockout mice or various Plexins (PlexA2, A4, or D1)-knockdown cortical neurons. These results strongly support the importance of the TRX-CRMP2 interaction in Sema3A signaling, which is consistent with the results obtained from the growth cone collapse assays.

3.3.3. TRX reduces disulfide-linked CRMP2 homodimer induced by Sema3A

I next examined the redox state of CRMP2 using IAA treatment and non-reducing SDS-PAGE. Along with signals corresponding to monomeric FLAG-CRMP2 at 65-kDa, signals around 135-kDa were also detected by anti-FLAG antibody in response to H₂O₂ treatment (Figure 11A). These signals were not apparent when SDS-PAGE was conducted under conventional reducing conditions. Thus, the 135-kDa signals are thought to reflect some disulfide-linked oligomeric form of FLAG-CRMP2. In addition, this oligomer formation seems to occur inside cells, because IAA treatment of cell lysates completely blocked *in vitro* formation of FLAG-CRMP2 oligomer by H₂O₂, thus excluding the possibility of artificial oligomer formation after harvesting cells *in vitro* (Figure 11B). This H₂O₂-induced CRMP2 oligomer formation was dependent on the presence of Cys504 because the FLAG-CRMP2 C504S sample did not show a 135-kDa signal (Figure 11A). To investigate the involvement of other cysteine residues in CRMP2, I co-expressed Myc-CRMP2 WT and FLAG-CRMP2 C504S and found that

Myc-CRMP2 WT did not form disulfide-linked oligomer with FLAG-CRMP2 C504S (Figure 11C), showing that only Cys504 is involved in disulfide bond formation. I next examined whether endogenous CRMP2 in DRG neurons can also form the homodimer in response to the presence of H₂O₂. I detected the presence of H₂O₂-induced homodimer (Figure 11D), as ectopically expressed FLAG-CRMP2. Next, I analyzed the effect of TRX on the disulfide bond of CRMP2. I first performed an *in vitro* reduction assay. COS-7 cells expressing FLAG-CRMP2 were stimulated with H₂O₂, and then FLAG-CRMP2 was purified with anti-FLAG beads and incubated with His-TRX. In the presence of His-TRX WT, FLAG-CRMP2 was reduced as opposed to that mixed with His-TRX C32/35S (Figure 12A), showing that TRX can reduce the disulfide bonds *in vitro*. Moreover, co-expression of Myc-TRX WT or C35S reduced the amount of H₂O₂-induced homodimer of FLAG-CRMP2 in cells (Figure 12B). I also investigated the effects of TRX-knockdown on CRMP2 oxidation and found that TRX siRNA augmented CRMP2 oxidation (Figure 12C), thus confirming that TRX is involved in reduction of CRMP2 *in vivo*. Treatment with DNCB also resulted in CRMP2 oxidation.

Next, I examined whether H₂O₂ is generated by Sema3A treatment in DRG neurons based on the fact that MICAL, which is involved in Sema signaling in both *Drosophila* and mammalian cells (20, 21), can generate H₂O₂ (21, 22). I utilized the recently developed H₂O₂-specific probe, GFP-HyPer to monitor H₂O₂ generation by Sema3A (37). The H₂O₂ treatment of HyPer-transfected DRG neurons resulted in augmentation of fluorescence in neurites (Figure 13A). Sema3A treatment also increased fluorescence at the tips of neurites. Thus, I chose to examine the oxidation of CRMP2 resulting from Sema3A treatment, and succeeded in detecting the presence of a CRMP2 homodimer in response to Sema3A treatment (Figure 13B).

3.3.4. Sema3A stimulates H₂O₂ generation via MICAL

I next examined the mechanism of Sema3A-induced H₂O₂ generation. Although MICAL is a plausible candidate, whether it is involved in Sema3A-induced H₂O₂ generation remained uncertain. There are three MICAL isoforms (MICAL1, 2, and 3) in mammals (20, 23). RT-PCR analyses indicated that MICAL1 and 3 are significantly expressed in DRG neurons but I could detect only a little expression of MICAL2 (Figure 14A). Thus, I transfected DRG neurons with siRNAs against both MICAL1 and 3, and confirmed the decreased expression of their cognate mRNAs (Figure 14B). I then evaluated the fluorescence of HyPer in the MICAL-knockdown neurons and found that the fluorescence did not increase in response to Sema3A in contrast to control cells (Figure 14C), indicating that endogenous MICAL is responsible for Sema3A-dependent H₂O₂ generation. To exclude the possibility of the off-target effects, I performed rescue experiments using a mouse MICAL1 construct that is resistant to siRNAs against rat MICAL1 and 3 (Figure 14C and 15B). DRG neurons transfected with FLAG-mMICAL1 together with siRNAs against MICAL showed normal H₂O₂ production in response to Sema3A. In contrast, mMICAL1 GW, which is catalytically inactive (20), failed to restore H₂O₂ production. These results convincingly indicate that Sema3A stimulates H₂O₂ generation via MICAL. Next, I examined the effect of MICAL-knockdown on the oxidation state of CRMP2. As expected, CRMP2 in MICAL-knockdown neurons did not form the disulfide-linked homodimer in response to Sema3A stimulation (Figure 14D).

I also observed the morphology of the growth cones in MICAL-knockdown neurons. Neurons transfected with siRNA against either MICAL1 or MICAL3 showed

moderate reduction in the rate of growth cone collapse (Figure 15A). Furthermore, neurons transfected with both MICAL1 and MICAL3 siRNAs showed a severer defect in growth cone collapse (Figure 15A). Again, I confirmed that the expression of FLAG-mMICAL1 rescued the defect in collapse response (Figure 15B). These results clearly confirm the importance of mammalian MICAL for Sema3A signaling.

3.3.5. TRX mediates oxidation-dependent CRMP2 phosphorylation

Having established the conditions for the oxidation of CRMP2, I then wanted to understand what impact the CRMP2 oxidation had on the cells. When cells expressing FLAG-CRMP2 were treated with H₂O₂, I noticed that a small amount of the FLAG-CRMP2 band shifted upward (Figure 16). As a similar mobility shift is known to occur during Sema3A signaling by GSK3-dependent phosphorylation which is important for Sema3A-induced growth cone collapse (16, 17, 19), I examined whether H₂O₂-induced CRMP2 phosphorylation occurs at the site phosphorylated by GSK3. Western blot analyses using an antibody specifically recognizing GSK3-phosphorylated CRMP2 (p-CRMP2) (19) revealed that H₂O₂-induced CRMP2 phosphorylation occurs at the GSK3 site (Figure 16). Similar phosphorylation of endogenous CRMP2 was also observed when DRG neurons were treated with H₂O₂ (Figure 17A). Next, I assessed the importance of TRX in H₂O₂-induced CRMP2 phosphorylation. Unexpectedly, co-expression of Myc-TRX WT or C35S rather enhanced phosphorylation whereas Myc-TRX C32/35S repressed (Figure 16). Moreover, Myc-TRX was less effective in the case of FLAG-CRMP2 C504S, although enhancement was still observed. These results suggest that TRX plays a positive role in CRMP2 phosphorylation. To confirm this possibility, I performed RNAi-knockdown experiments of TRX, which resulted in

significant inhibition of CRMP2 phosphorylation (Figure 17B). I also found that Myc-CRMP2 C504S expressed in neurons was less phosphorylated than Myc-CRMP2 WT when treated with Sema3A (Figure 17C).

Having confirmed TRX-mediated CRMP2 phosphorylation, I conducted GST pull-down assays to investigate the effects of the phosphorylation on the CRMP2 function. Mouse brain lysates or purified tubulin proteins were subjected to pull-down assays with CRMP2-GST WT or T514D, which mimics GSK3 β -phosphorylated CRMP2 (19), and the precipitates were examined by immunoblotting analyses for known CRMP2-binding proteins, such as tubulin, Numb, KLC1, actin, DHC, and Slp1 (18, 38-42). As shown in Figure 18, the T514D mutation significantly weakened the interaction with tubulin and Numb, but not actin, as reported previously (19, 43). Moreover, the amounts of KLC1 and Slp1 associated with CRMP2-GST were also found to be decreased by the mutation, whereas those of DHC were not. Because it has been shown that CRMP2 regulates tubulin assembly and vehicle transportation on microtubules with Numb, KLC1, and Slp1 (18, 38, 39, 41), these results suggest that CRMP2 phosphorylation preferentially affects microtubule-dependent function by disrupting tubulin assembly and vehicle transportation.

3.3.6. The molecular mechanisms of TRX-mediated CRMP2 phosphorylation

These results point out an interesting possibility that CRMP2 phosphorylation is linked to complex formation between TRX and CRMP2. Indeed, immunoblotting analyses after non-reducing SDS-PAGE revealed that CRMP2 linked to TRX was more preferentially phosphorylated than the monomer or disulfide-linked homodimer (Figure 19A). This seems to be the reason that FLAG-TRX C35S showed no dominant negative

effect on growth cone collapse (Figure 7B).

Lastly, I tried to reconstitute the TRX-mediated augmentation of CRMP2 phosphorylation using purified recombinant proteins. CRMP2 was weakly phosphorylated by addition of CDK5, which is known to function as a priming kinase for GSK3-dependent CRMP2 phosphorylation (16, 17, 19), and GSK3 β (Figure 19B), as reported previously. Further addition of His-TRX alone showed no significant effect on CRMP2 phosphorylation not only in reduced (DTT) condition but also in oxidized (H₂O₂) condition. I speculated that only a small amount of His-TRX interacts with CRMP2, because His-TRX should be directly oxidized by H₂O₂ or rapidly released from CRMP2 by formation of an intramolecular disulfide bond. Therefore, I also added TxR and NADPH to regenerate His-TRX, and found that it significantly augmented CRMP2 phosphorylation only when the reaction was performed in the presence of H₂O₂. In addition, His-TRX C32/35S did not promote CRMP2 phosphorylation, and there was no stimulatory effect on the phosphorylation of CRMP2 C504S (Figure 19C). I then examined the phosphorylation by which kinase is stimulated by TRX. Kinase assays with ³²P-labelled ATP revealed that phosphorylation by GSK3 β was augmented by TRX in the presence of the TRX-regeneration system and H₂O₂ whereas phosphorylation by CDK5 was not (Figure 20, A and B). These results indicate that the disulfide-linked interaction between TRX and CRMP2 stimulates CRMP2 phosphorylation by GSK3 β .

3.4. Discussion

Here I showed an unexpected mechanism of H₂O₂-mediated signal transduction in Sema3A signaling. Upon Sema3A stimulation, MICAL generates H₂O₂ at growth cones and oxidizes CRMP2 to form a disulfide-linked homodimer through Cys504 (Figure 21). In turn, oxidized CRMP2 forms a disulfide complex with TRX and becomes preferentially phosphorylated by GSK3, resulting in growth cone collapse.

Several studies have elucidated key players in Sema3A-induced CRMP2 phosphorylation. It is reported that a tyrosine kinase Fyn associates with PlexA and phosphorylates CDK5 at Tyr15 (44), which augments its kinase activity. However, the mechanisms of both Fyn activation and CDK5 phosphorylation by Sema3A stimulation are unknown. In this point, it should be noted that my study clearly demonstrated H₂O₂ generation by MICAL. Accumulating evidence indicates that protein tyrosine phosphatases are susceptible to H₂O₂-induced oxidation, which generally results in inactivation of their phosphatase activity (2-5). Therefore, MICAL-generated H₂O₂ may also contribute to sustaining CDK5 activation through blockade of CDK5 inactivation by Tyr15 dephosphorylation.

On the other hand, it is reported that R-Ras-regulated pathway participates in CRMP2 phosphorylation by GSK3 (45, 46). Sema4D-activated PlexB functions as a GTPase-activating protein for R-Ras and inactivates it, resulting in inhibition of Akt. Akt is known to inactivate GSK3 via phosphorylation of Ser9 in GSK3, and thus Sema4D stimulation ultimately induces GSK3 activation. In contrast, my results shown in Figure 17 to 20 clearly demonstrate the crucial importance of CRMP2 oxidation for phosphorylation. Therefore, not only kinase activation but also substrate sensitization

(by oxidation) are important for CRMP2 phosphorylation. At least in my experimental settings utilizing Sema3A-stimulated DRG neurons, I observed no significant Akt inactivation or GSK3 activation (Figure 22). Collectively, CRMP2 phosphorylation appears to be regulated at multiple levels *in vivo*, which allows precise and complex regulation of CRMP2 in different cell types.

My study revealed that H₂O₂ is actually generated via MICAL by Sema3A treatment, which is crucial for CRMP2 oxidation and growth cone collapse. In consistent with these results, the importance of mammalian MICAL in Sema3A signaling was recently reported (21). In the paper, it was also shown that CRMP directly binds to the monooxygenase domain of MICAL, raising an interesting possibility that CRMP2 might be directly oxidized by MICAL. Certain kinds of flavoprotein monooxygenases catalyze oxidation of various thiol compounds such as cysteamine, cysteine, and a tripeptide glutathione to form disulfide bonds (47, 48). In addition, a structural analysis suggests that the monooxygenase domain of MICAL requires the binding of macromolecules, such as polypeptides, to be stabilized and the authors propose proteins to be substrates (49). Therefore, the complex formation between MICAL and CRMP2 may accelerate the oxidation efficiency of CRMP2.

Cys504 is placed at the C-terminal tail region in CRMP2, in which many phosphorylation sites also exist. This tail region was predicted to be unfolded (50, 51). Thus, the association of TRX at Cys504 would not prevent GSK3 from interacting with these phosphorylation sites, because the phosphorylation target Ser residues can rotate rather freely in the unfolded polypeptide. It would be interesting to solve the 3-D structure of the TRX/CRMP2 disulfide complex. Alternatively, TRX may recruit GSK3 β to its substrate CRMP2.

The Cys504 is conserved in all vertebrate CRMP2, but not in *C. elegans* or *D. melanogaster* (Figure 23). Moreover, the C-terminal region including Cys504 is also rarely conserved in these simpler organisms. This region is predicted to be unfolded (50, 51), and thus, I suppose that other Cys residues in *C. elegans* or *D. melanogaster* might compensate the function of the Cys504 in vertebrates. It should also be noted that the phosphorylation sites for both GSK3 β and CDK5 (Thr509, Thr514, Ser518 and Ser522 in human CRMP2) are also not conserved in *C. elegans* or *D. melanogaster*, but I can find the corresponding residues in all vertebrate CRMP2. Therefore, there is another possibility that CRMP2 oxidation and phosphorylation have evolved to emerge simultaneously around the advent of vertebrates, to connect MICAL-generated H₂O₂ to CRMP2 phosphorylation.

It has been indicated that the CRMP proteins form an oligomer by themselves (52). In the protein complex composed of CRMP2 WT and C504S, CRMP2 WT is supposed not to be able to form a disulfide bridge with CRMP2 C504S. When CRMP2 C504S is ectopically expressed, the amount of CRMP2 C504S should be much larger than that of endogenous (WT) CRMP2, and thus, most endogenous CRMP2 is presumably trapped in the complex with CRMP2 C504S. Under such condition, endogenous CRMP2 cannot form a disulfide bridge. I think that this is the reason why ectopically expressed CRMP2 C504S dominant-negatively inhibits the Sema3A-induced growth cone collapse.

3.5. Figures

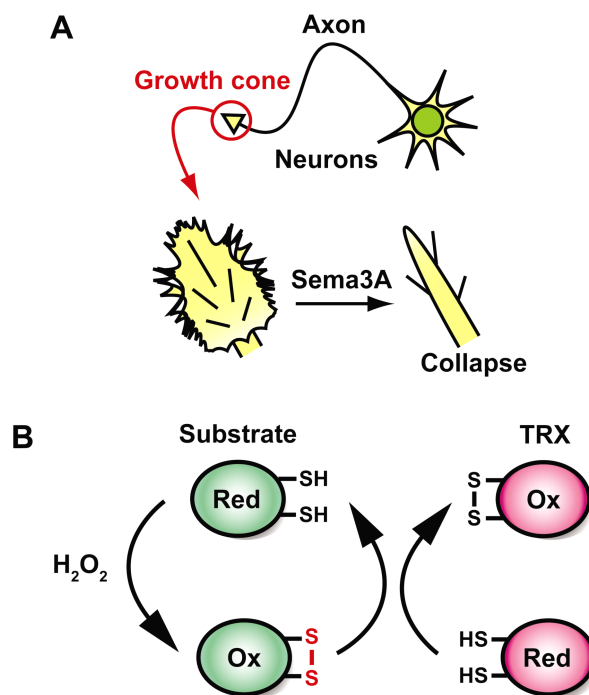
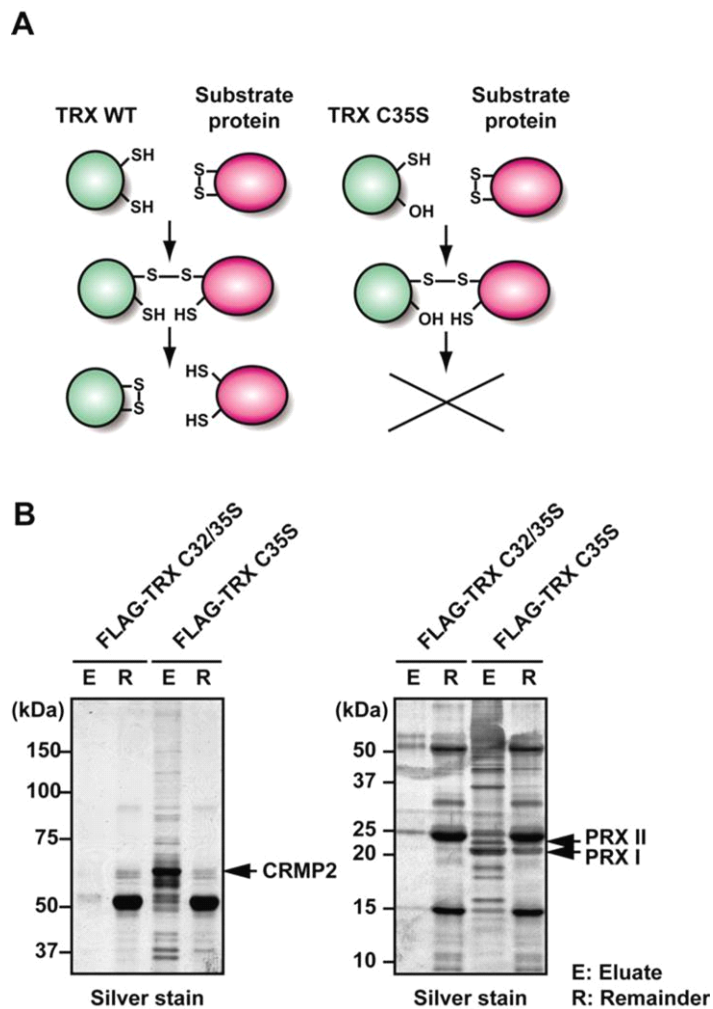


Figure 1. The models of the redox regulation and growth cone collapse.

(A) The schematic model of the redox regulation of protein. Reduced (Red) protein is oxidized by H_2O_2 and oxidized (Ox) protein is reduced by TRX.

(B) The schematic model of Sema3A-induced growth cone collapse.



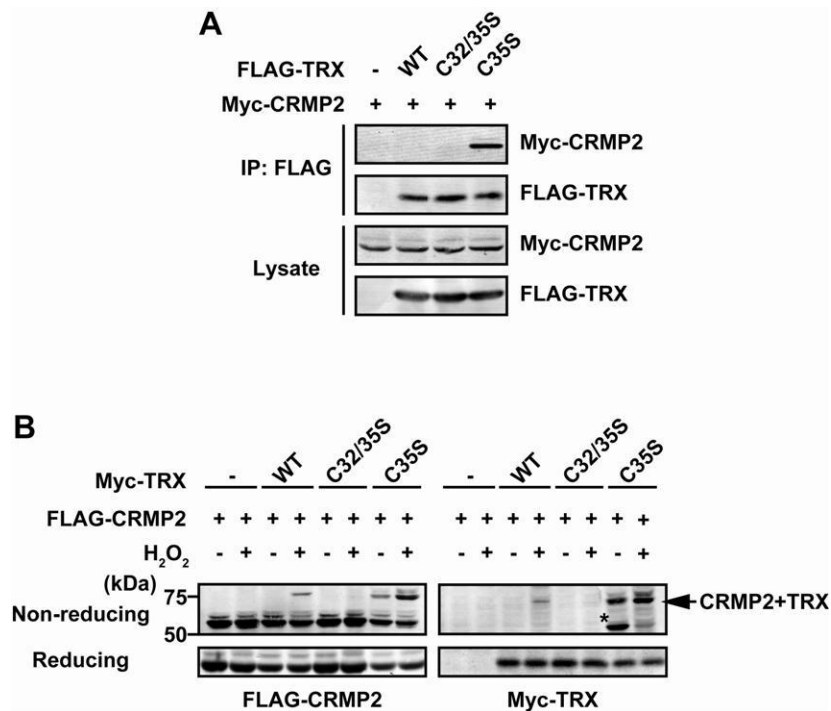


Figure 3. The interaction between TRX and CRMP2.

(A) Lysates from COS-7 cells transfected with the indicated constructs were immunoprecipitated (IP) with anti-FLAG antibodies and analyzed by immunoblotting.

(B) COS-7 cells were transfected with the indicated constructs and treated with 100 μ M H₂O₂ for 5 min. Cell lysates were treated with IAA and immunoblotted under non-reducing and reducing conditions. Asterisk (*) indicates the signal of TRX C35S that formed a complex with an unidentified protein.

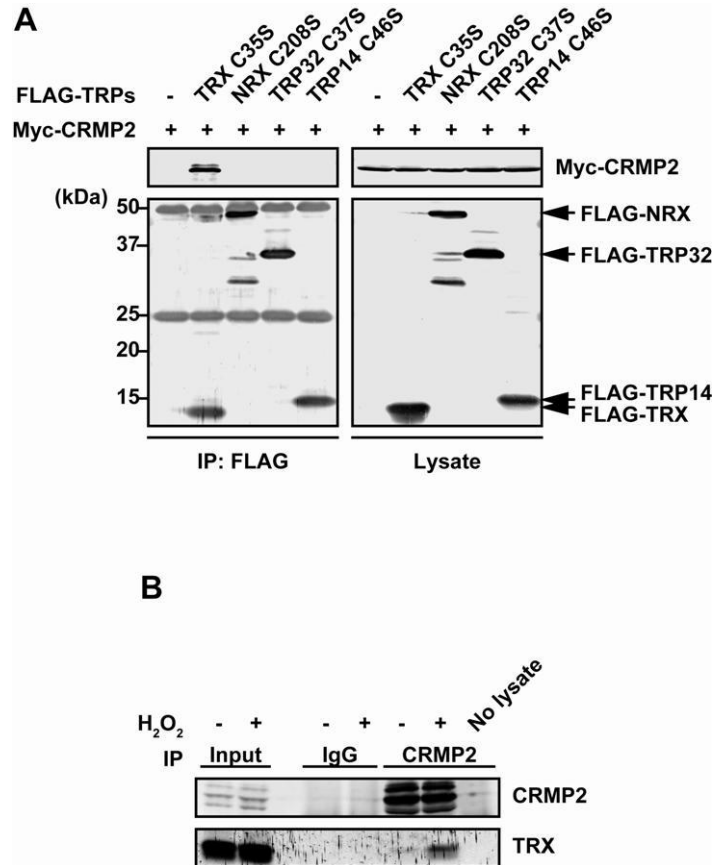


Figure 4. Specificity of TRX-CRMP2 interaction.

(A) Lysates from COS-7 cells transfected with the indicated constructs were immunoprecipitated (IP) with anti-FLAG antibodies and analyzed by immunoblotting.

(B) Lysates of N1E-115 neuroblastoma cells treated with 500 μ M H₂O₂ for 5 min were treated with IAA, acetone precipitated and dissolved. They were then immunoprecipitated with anti-CRMP2 antibodies and immunoblotted with indicated antibodies.

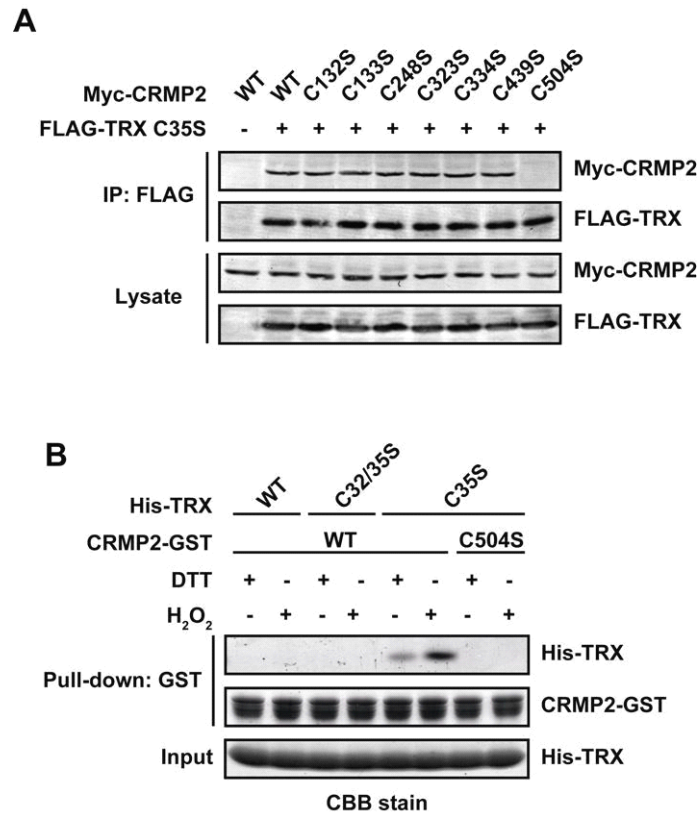


Figure 5. Cys504 is necessary for CRMP2 to interact with TRX.

(A) Lysates from COS-7 cells transfected with the indicated constructs were immunoprecipitated (IP) with anti-FLAG antibodies and analyzed by immunoblotting.

(B) GST-CRMP2 pull-down assays of recombinant His-TRX in the presence of 5 mM DTT or 100 μ M H₂O₂. Proteins were subjected to SDS-PAGE and CBB-staining.

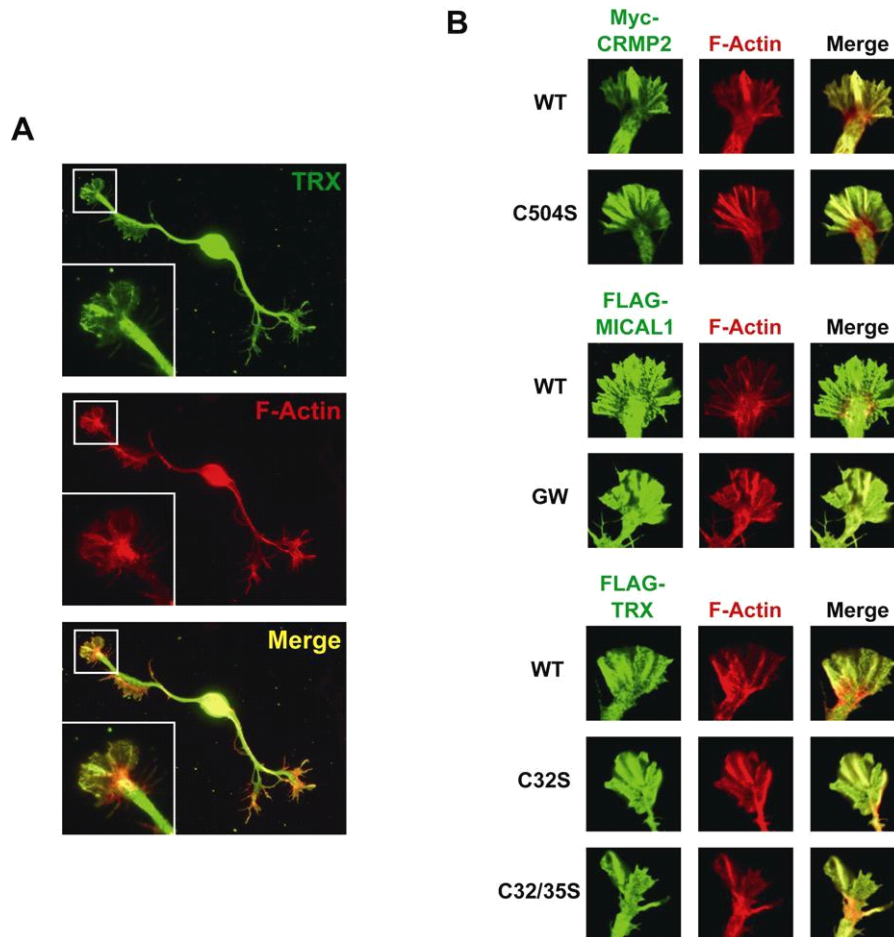


Figure 6. Immunolocalization of endogenous TRX and ectopically expressed proteins in growth cones.

(**A**) DRG neurons were stained with anti-TRX antibody (green) and phalloidin to visualize actin filaments (red).

(**B**) DRG neurons were transfected with the indicated constructs and subjected to immunocytochemical staining with indicated antibodies (green) and phalloidin (red).

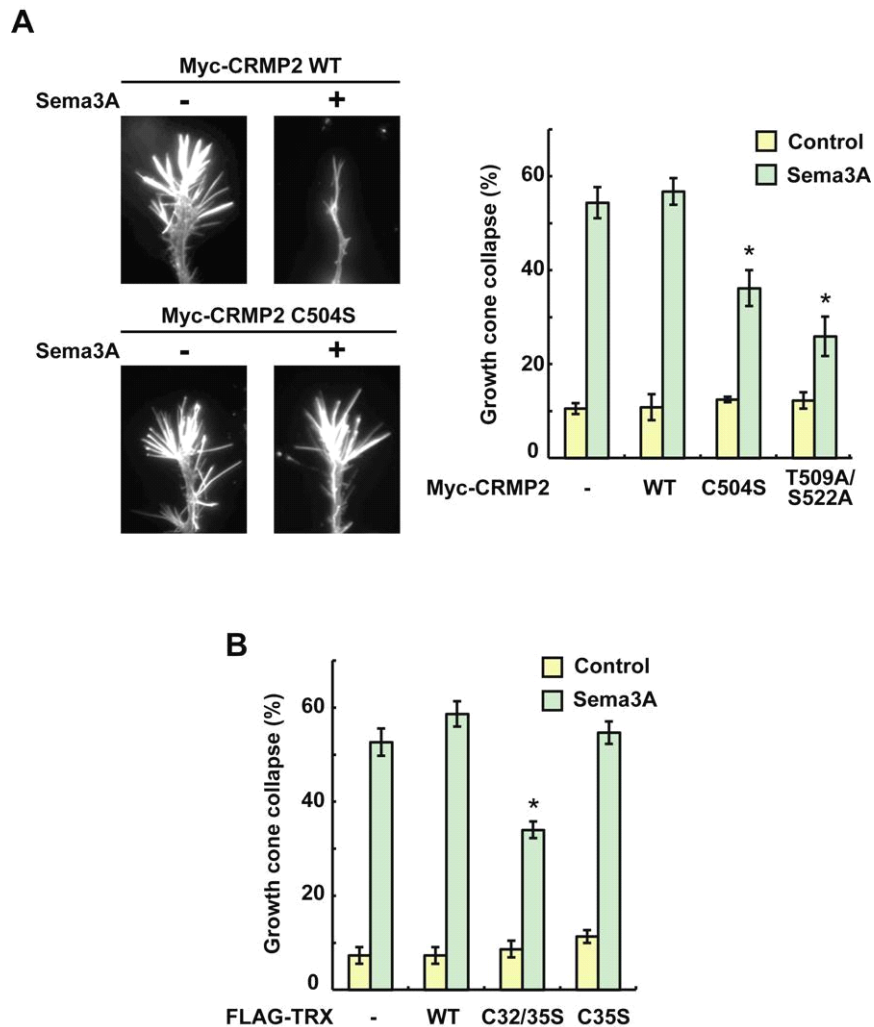


Figure 7. Crucial importance of TRX-CRMP2 interaction in Sema3A-induced growth cone collapse.

(**A** and **B**) DRG neurons were transfected with the indicated constructs together with the GFP-expressing plasmid. Sema3A-treated (30 min) cells were fixed and stained with phalloidin. GFP-positive cells were examined. Data are mean \pm SEM (n = 3-4). Asterisks (*) indicate significant difference ($p < 0.05$) from the control. Typical images of growth cones are also shown (A).

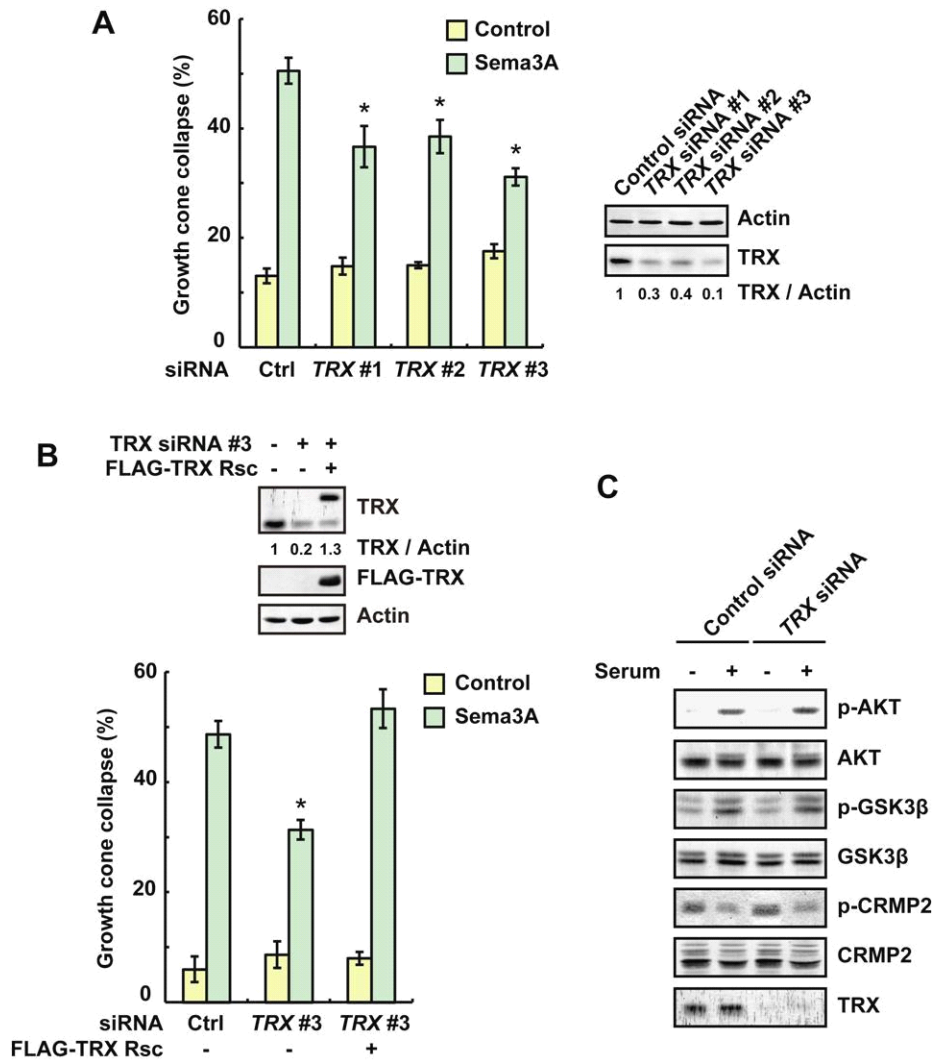


Figure 8. Crucial importance of TRX in Sema3A-induced growth cone collapse.

(**A** and **B**) DRG neurons were transfected with the indicated constructs or siRNAs for TRX together with the GFP-expressing plasmid. Sema3A-treated (30 min) cells were fixed and stained with phalloidin. GFP-positive cells were examined. Data are mean \pm SEM (n = 3-4). Asterisks (*) indicate significant difference (p < 0.05) from the control. Knockdown efficiencies by TRX siRNAs with quantification are also shown.

(**C**) DRG neurons were transfected with the indicated siRNAs. After 3 hours of starvation, they were stimulated with serum for 30 minutes and analyzed by immunoblotting with indicated antibodies.

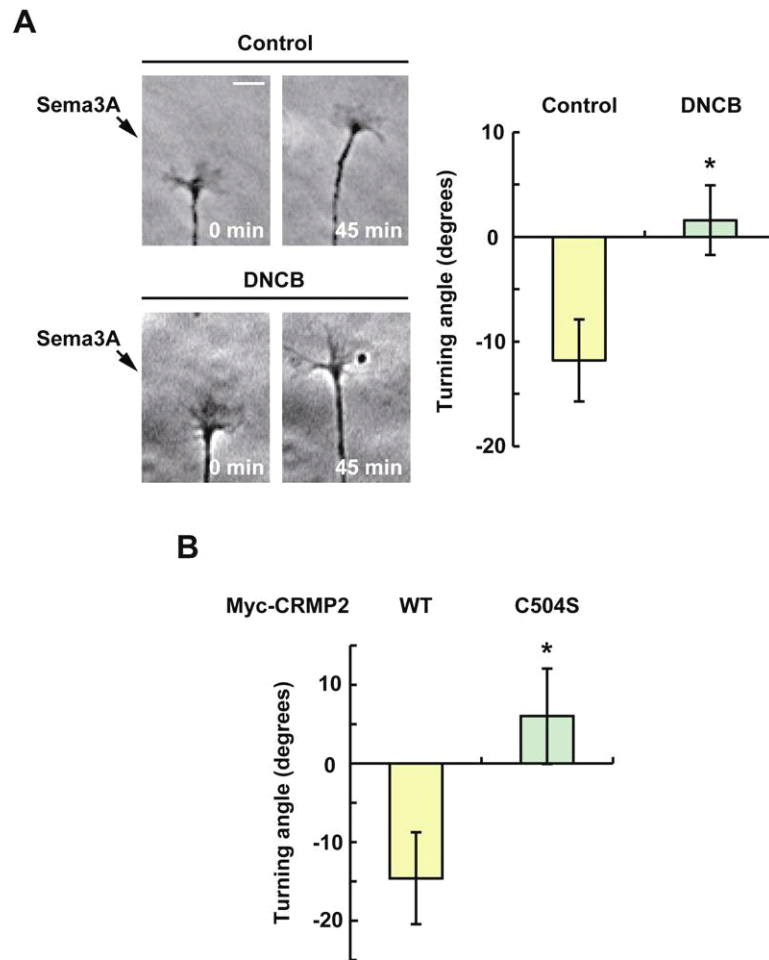


Figure 9. Crucial importance of TRX-CRMP2 interaction in Sema3A-guided growth cone turning.

(A) Time-lapse phase-contrast images of chicken DRG growth cones exposed to Sema3A gradients (arrows) in the absence (control) or presence of 10 μ M DNCB. Digits represent minute after the onset of Sema3A application.

(B) Chicken growth cones transfected with the indicated constructs were exposed to Sema3A gradients.

(A and B) Graphs show turning angle of growth cones (mean \pm SEM, n = 12-15), with positive and negative values indicating attraction and repulsion, respectively. Asterisks (*) indicate significant difference (p < 0.05) from the control growth cones.

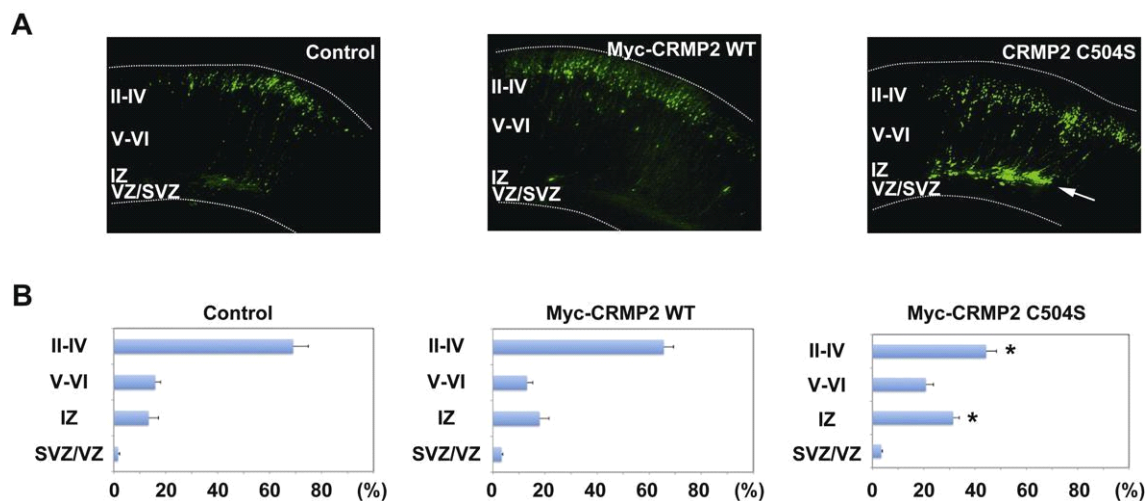


Figure 10. Crucial importance of TRX-CRMP2 interaction in the radial migration of cortical neurons.

(A) Embryonic brains at E14.5 were electroporated with the indicated constructs plus GFP, followed by fixation at P0. Frozen sections were examined. White dotted lines represent pial and ventricular surfaces. A white arrow indicates abnormal accumulation of cells in the IZ. Scale bar, 200 μ m.

(B) Data are mean \pm SEM (n = 5). Asterisks (*) indicate significant difference ($p < 0.05$) from the control. II-IV, layers II-IV of the cortical plate; V-VI, layers V-VI of the cortical plate; IZ, intermediate zone; VZ, ventricular zone; SVZ, subventricular zone.

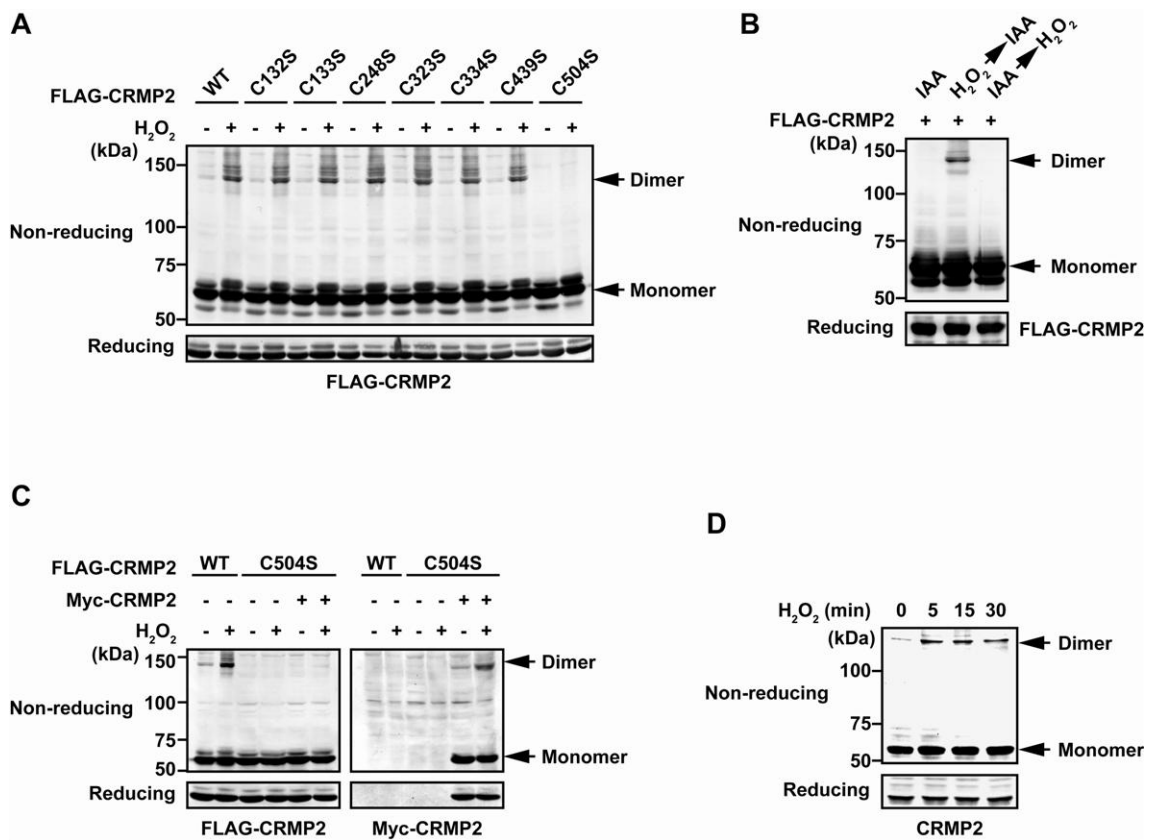


Figure 11. CRMP2 forms disulfide-linked homodimer.

(**A** and **C**) COS-7 cells were transfected with the indicated constructs and then treated with 100 μ M H₂O₂ for 5 min. Cell lysates were treated with IAA and immunoblotted under non-reducing and reducing conditions.

(**B**) Lysates from COS-7 cells transfected with the FLAG-CRMP2-expressing plasmids were treated with H₂O₂ either before or after IAA treatment and immunoblotted under non-reducing and reducing conditions.

(**D**) DRG neurons were treated with 100 μ M H₂O₂ for indicated times and analyzed with anti-CRMP2 immunoblotting.

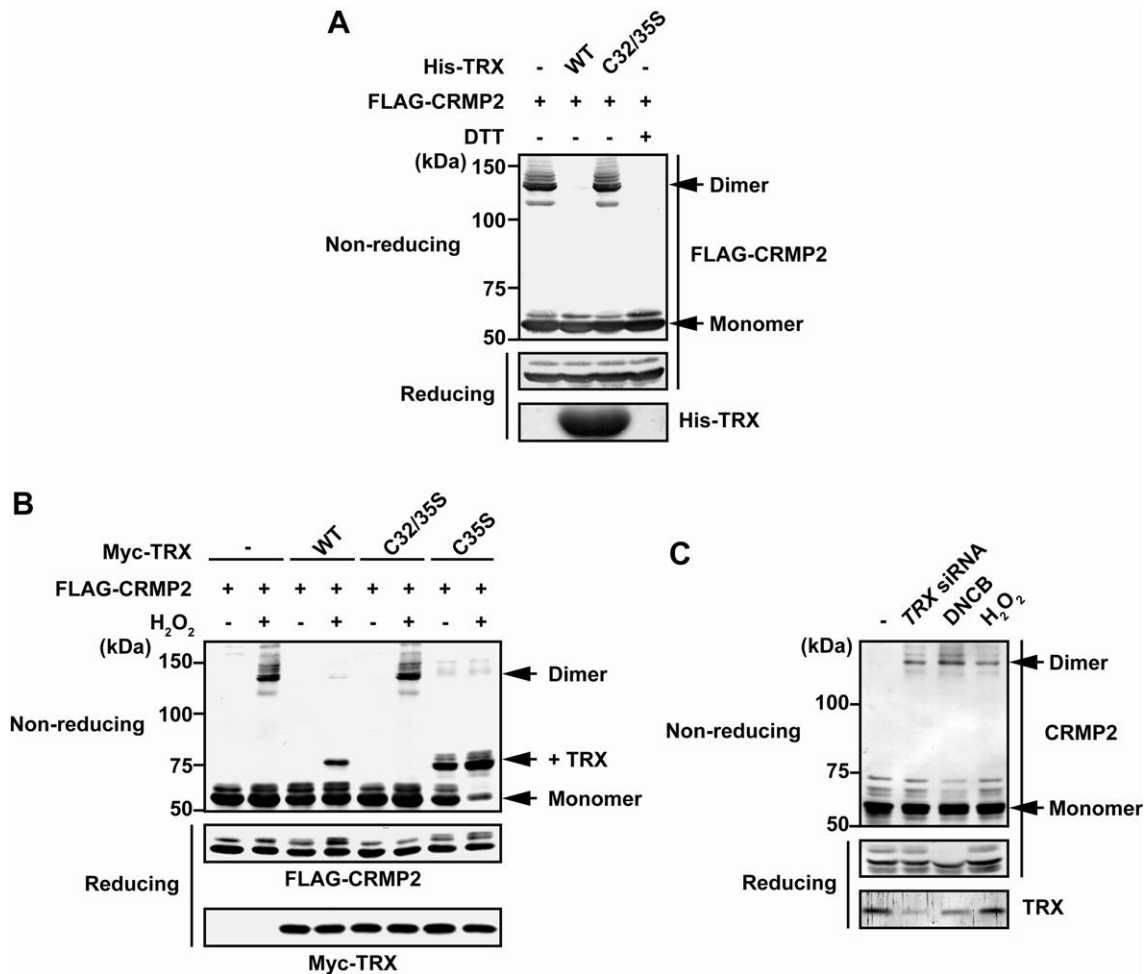


Figure 12. TRX reduces disulfide-linked CRMP2 homodimer.

(A) Lysates of H₂O₂-treated COS-7 cells expressing FLAG-CRMP2 were immunoprecipitated with anti-FLAG antibody. The immunoprecipitates were incubated with His-TRX or DTT, and then analyzed with anti-FLAG immunoblotting.

(B) COS-7 cells were transfected with the indicated constructs and then treated with 100 μM H₂O₂ for 30 min. Cell lysates were treated with IAA and immunoblotted under non-reducing and reducing conditions.

(C) DRG neurons transfected with TRX siRNA or treated with DNCB (100 μM for 60 min) or H₂O₂ (100 μM for 5 min) were analyzed with anti-CRMP2 immunoblotting.

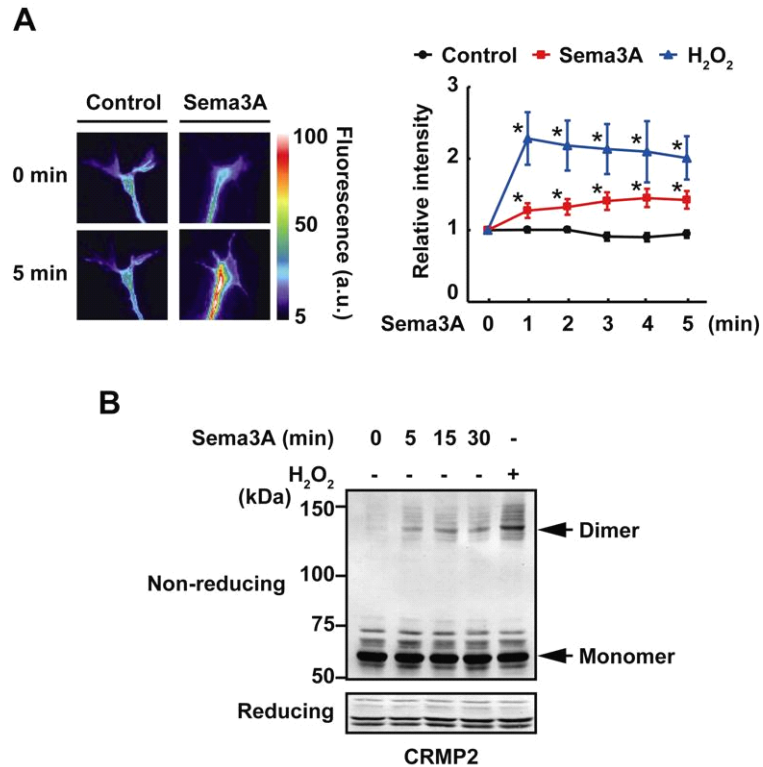


Figure 13. Sema3A induces H₂O₂ generation and CRMP2 oxidation.

(A) DRG neurons were transfected with GFP-HyPer plasmid and then stimulated with Sema3A or 100 μ M H₂O₂. Pseudo-colored images and calibration bars (arbitrary unit) are indicated. Relative intensity in growth cones was analyzed. Data are mean \pm SEM. For each construct, 5-8 neurons were measured. Asterisks (*) indicate significant difference ($p < 0.05$) from the control.

(B) DRG neurons were stimulated with Sema3A for indicated times and analyzed with anti-CRMP2 antibody.

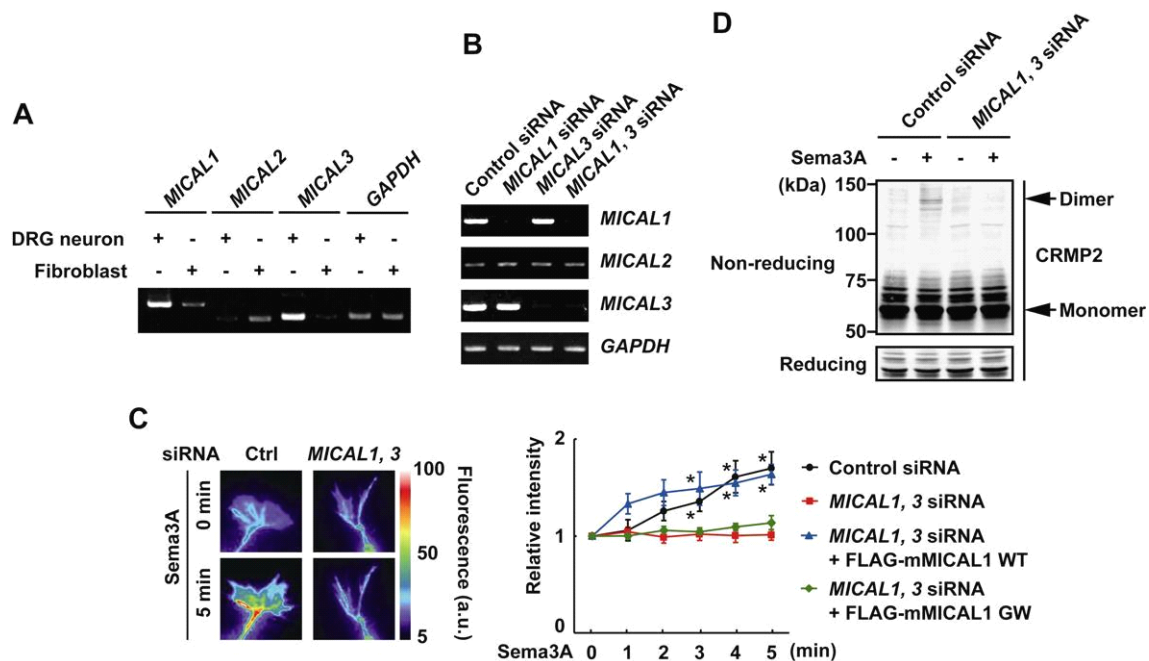


Figure 14. MICAL regulates Semaphorin 3A-induced H₂O₂ generation and following CRMP2 oxidation.

(A) RT-PCR analyses of MICAL1-3 were performed.

(B) DRG neurons were transfected with the indicated siRNAs and then subjected to RT-PCR analyses for each MICAL isoform.

(C) DRG neurons were transfected with the indicated siRNAs and constructs, together with the GFP-HyPer plasmid, and then stimulated with Semaphorin 3A. Representative fluorescent images are pseudo-colored and shown with a calibration bar (left panel. a.u.: arbitrary unit). Relative intensity of GFP fluorescence in the growth cones are presented as mean \pm SEM (Right panel. 6 neurons for each construct). Asterisks (*) indicate significant differences against control cells ($p < 0.05$).

(D) DRG neurons transfected with siRNAs for both MICAL1 and 3 were stimulated with Semaphorin 3A for 15 min. Lysates were treated with IAA and analyzed by immunoblotting with anti-CRMP2 antibody.

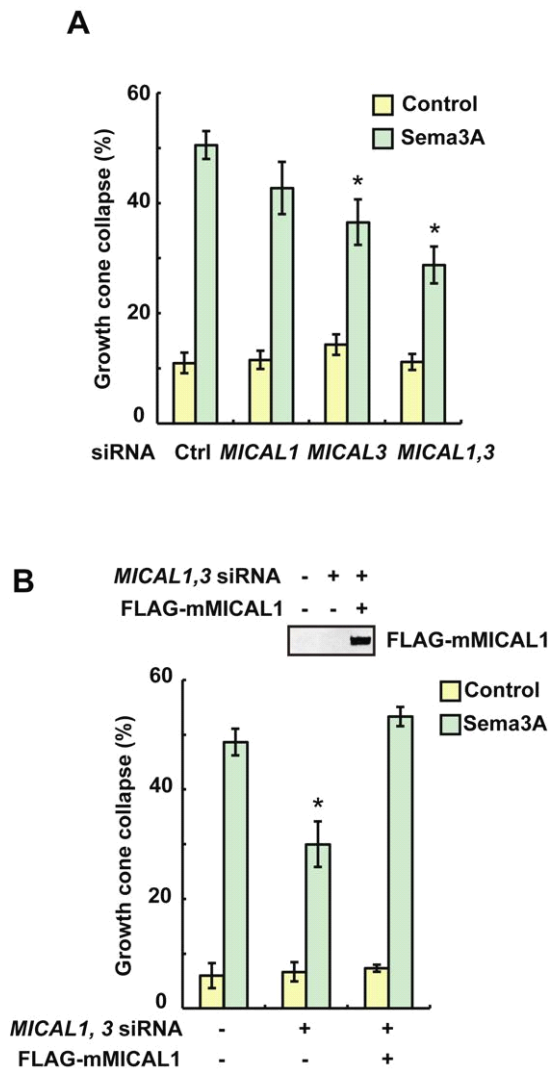


Figure 15. Crucial importance of MICAL in Sema3A-induced growth cone collapse.

(**A** and **B**) DRG neurons were transfected with the indicated constructs or siRNAs with the GFP-expressing plasmid. After treatment with Sema3A for 30 min, the cells were fixed and stained with phalloidin to visualize growth cones. Data are mean \pm SEM ($n = 3$). For each experiment, more than 50 GFP-positive neurons were measured. *: significant differences against control siRNA-transfected neurons ($p < 0.05$).

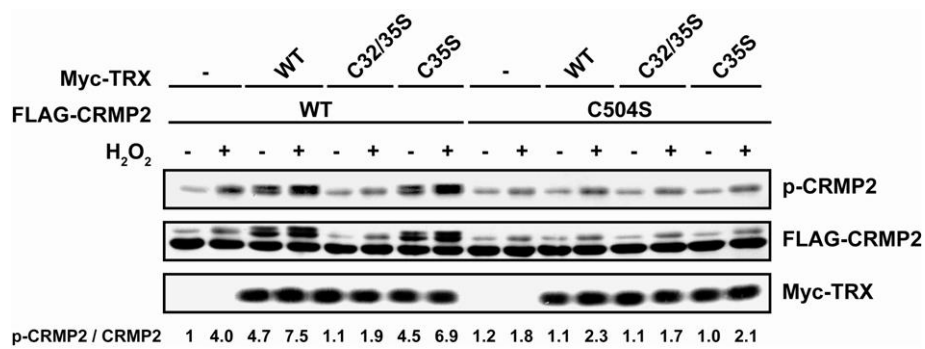


Figure 16. TRX promotes oxidation-dependent CRMP2 phosphorylation.

COS-7 cells were transfected with the indicated constructs and then treated with 100 μ M H₂O₂ for 15 min. Cell lysates were subjected to immunoblotting analyses.

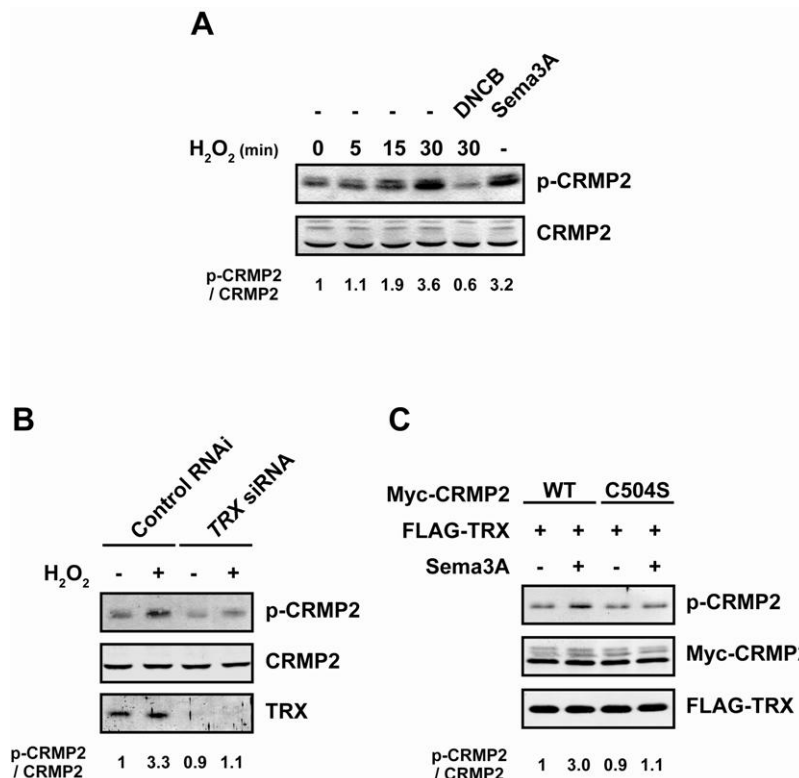


Figure 17. TRX mediates oxidation-dependent CRMP2 phosphorylation in neurons.

(A) DRG neurons were treated with 100 μ M H₂O₂ for indicated times or stimulated with Sema3A, and the cell lysates were subjected to immunoblotting.

(B and C) DRG neurons were transfected with indicated siRNAs or constructs and then stimulated with 100 μ M H₂O₂ or Sema3A, the cell lysates were analyzed with indicated antibodies.

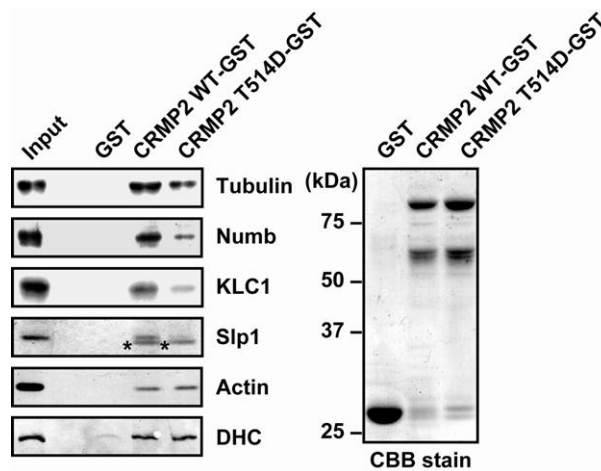


Figure 18. The effects of the phosphorylation on the CRMP2 function.

CRMP2-GST pull-down assays of mouse brain lysates or purified tubulin. Proteins were subjected to immunoblotting and CBB-staining. Asterisk (*) indicates the non-specific signal derived from CRMP2-GST, which reacted with anti-Slp1 antibody.

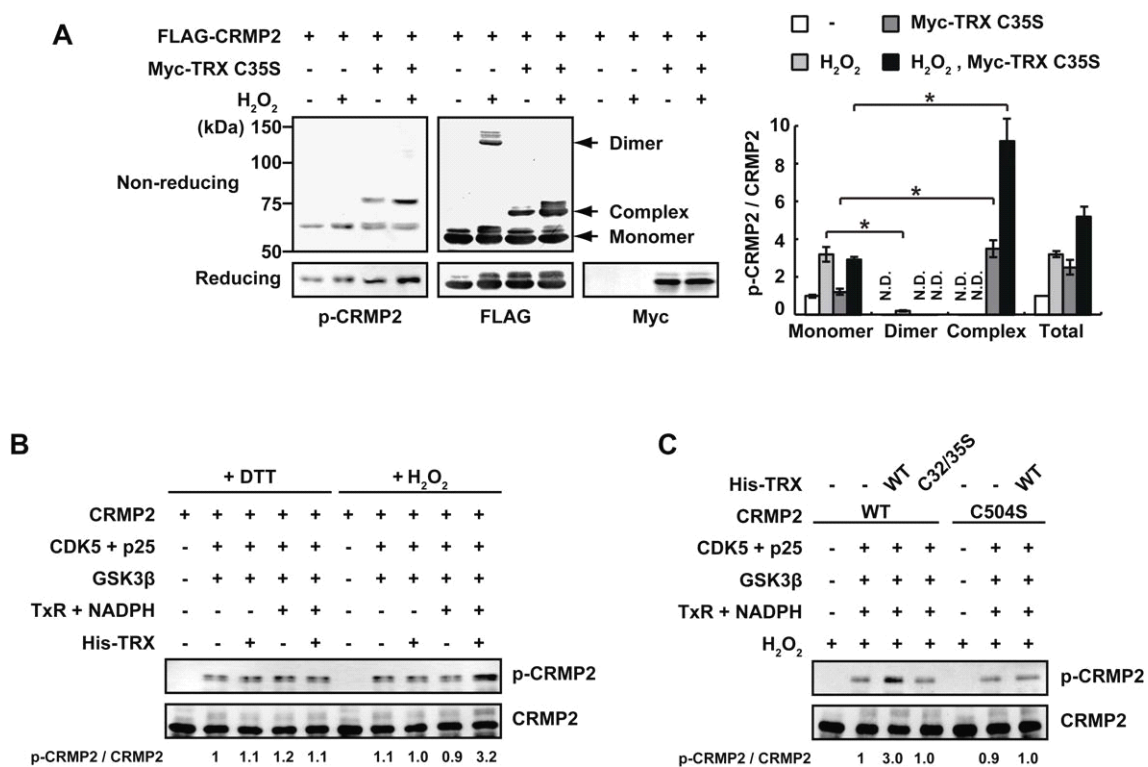


Figure 19. The molecular mechanisms of TRX-mediated CRMP2 phosphorylation.

(A) COS-7 cells transfected with the indicated constructs were treated with 100 μ M H₂O₂ for 15 min and subjected to immunoblotting under non-reducing and reducing conditions. Quantitative measurements of band intensities (p-CRMP2/CRMP2 of the monomer, dimer, complex with TRX, and total) with normalization are also shown. Data are mean \pm SEM (n = 3). *p < 0.01.

(B and C) *In vitro* kinase assays were performed using indicated recombinant proteins in the presence of DTT (5 mM) or H₂O₂ (100 μ M). Proteins were analyzed with indicated antibodies. Quantitative measurements of band intensities (p-CRMP2/CRMP2) with normalization are shown.

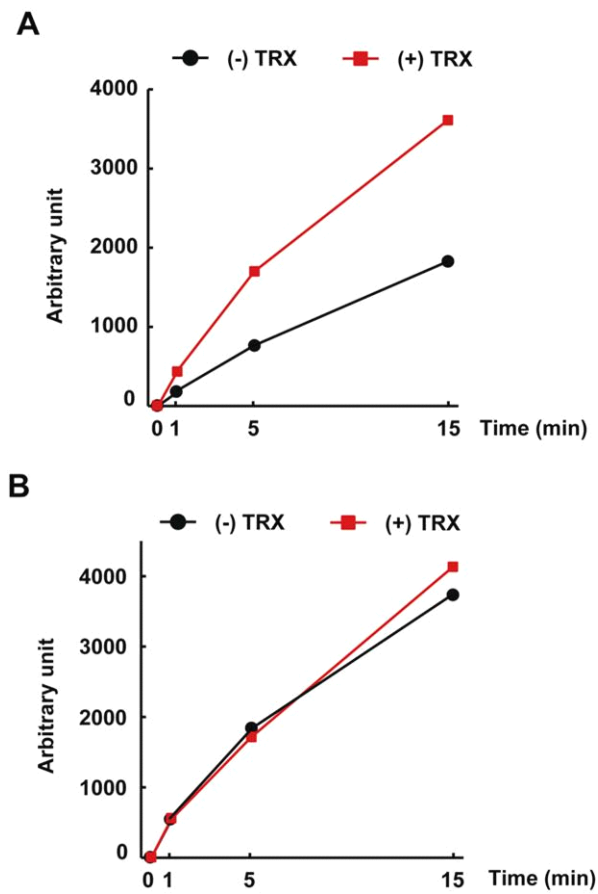


Figure 20. TRX promotes GSK3 β -dependent CRMP2 phosphorylation *in vitro*.

(A) Recombinant CRMP2 pre-phosphorylated by CDK5 was incubated with TxR, NADPH, H₂O₂ and GSK3 β in the presence of [γ -³²P]ATP for the time indicated. His-TRX was also added (red squares) or excluded (black circles). Proteins were then subjected to SDS-PAGE and autoradiography. Radioactivity of CRMP2 at each time point was determined and is presented as a graph.

(B) Recombinant CRMP2 was subjected to a kinase assay with CDK5/p25 as described in (A).

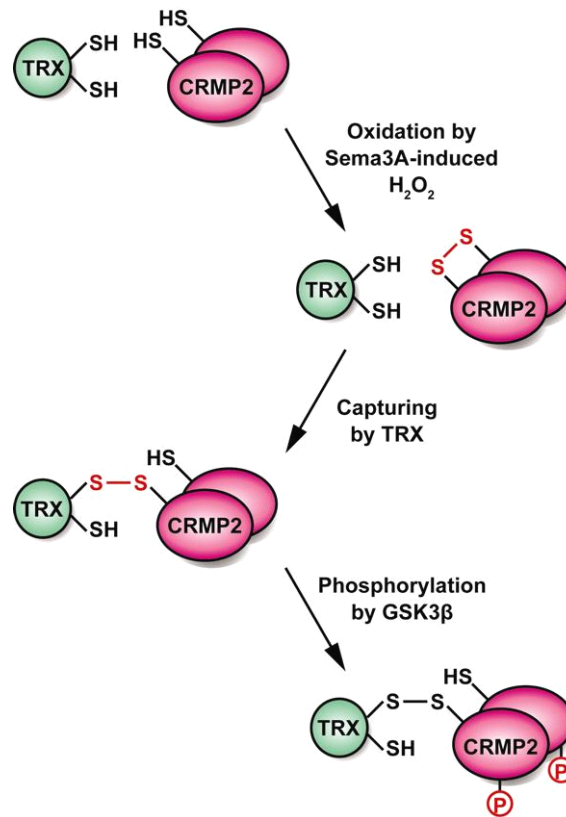


Figure 21. Model of TRX-mediated CRMP2 phosphorylation.

Upon Sema3A stimulation, MICAL generates H_2O_2 at growth cones and oxidizes CRMP2 to form a disulfide-linked homodimer through Cys504. In turn, oxidized CRMP2 forms a disulfide complex with TRX and becomes preferentially phosphorylated by GSK3, resulting in growth cone collapse.

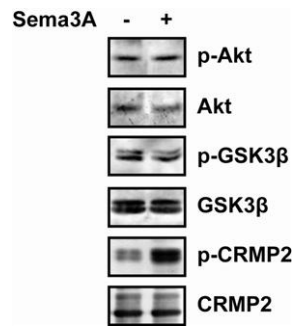


Figure 22. Sema3A stimulation does not alter Akt and GSK3 β phosphorylation.

DRG neurons were stimulated with Sema3A for 30 minutes and analyzed by immunoblotting with indicated antibodies.

| | | | Cys504 | Thr509 | Thr514 | Ser522 | | | |
|-----------------|-------|------------------------------------|--------|--------|--------|--------|------|------|-----|
| | | | ▼ | ▼ | ▼ | ▼ | | | |
| H. sapiens | : 497 | GLYDGPV | CEVSV | TPKTV | TPASS | SAKTS | ---- | PAKQ | 526 |
| M. musculus | : 497 | GLYDGPV | CEVSV | TPKTV | TPASS | SAKTS | ---- | PAKQ | 526 |
| R. rattus | : 497 | GLYDGPV | CEVSV | TPKTV | TPASS | SAKTS | ---- | PAKQ | 526 |
| X. laevis | : 497 | GLYDGPV | CEVSV | TPKAV | TPASS | SAKTS | ---- | PAKQ | 526 |
| D. rerio | : 497 | GLYDGPV | CEVSV | TPKAV | TPASS | SAKTS | ---- | PAKQ | 526 |
| D. melanogaster | : 504 | GSMAKRFAELDIQIPVQEPISAMLAGNLAMPAEG | | | | | | | 538 |
| C. elegans | : 801 | ASSQQQKPQQNGHHKNSGDFDRNRTK----- | | | | | | | 826 |

Figure 23. Alignment of the amino acid sequence of the region of human CRMP2 containing Cys504 with the corresponding sequences.

The human (*Homo sapiens*), mouse (*Mus musculus*), rat (*Rattus rattus*), frog (*Xenopus laevis*), zebrafish (*Danio rerio*), fruit fly (*Drosophila melanogaster*), and nematode (*Caenorhabditis elegans*) sequences are shown. Cys504, GSK3 β phosphorylation sites (Thr509, Thr514 and Ser518) and CDK5 phosphorylation sites (Ser522) are shown in red, blue and green respectively.

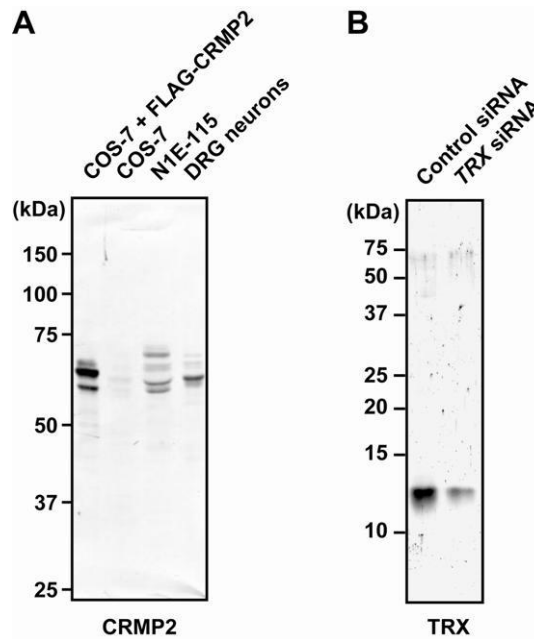


Figure 24. Characterization of the rabbit anti-CRMP2 antibody and the rabbit anti-TRX antibody.

(A) Lysates of indicated cells were subjected to immunoblotting analyses with the rabbit anti-CRMP2 antibody generated in this study.

(B) Lysates of DRG neurons transfected with the indicated siRNAs were subjected to immunoblotting analyses with the rabbit anti-TRX antibody used in immunocytochemical staining.

4.

**Oligomeric peroxiredoxin I is an essential intermediate
for p53 to activate MST1 kinase and apoptosis**

4.1. Abstract

MST1 kinase mediates H₂O₂-induced cell death by anticancer drugs such as cisplatin in a p53-dependent manner. However, the mechanism underlying MST1 activation by H₂O₂ remains unknown. Here I show that PRX I is an essential intermediate in H₂O₂-induced MST1 activation and cisplatin-induced cell death via p53. Cell stimulation with H₂O₂ resulted in PRX I oxidation to form homo-oligomers and interaction with MST1, leading to MST1 autophosphorylation and augmentation of kinase activity. In addition, RNAi-knockdown experiments indicated that endogenous PRX I is required for H₂O₂-induced MST1 activation. Live cell-imaging showed H₂O₂ generation by cisplatin treatment, which likewise caused PRX I oligomer formation, MST1 activation, and cell death. Cisplatin-induced PRX I oligomer formation was not observed in embryonic fibroblasts obtained from p53-knockout mice, confirming the importance of p53. Indeed, ectopic expression of p53 induced PRX I oligomer formation and cell death, both of which were cancelled by the antioxidant—NAC. Moreover, I succeeded in reconstituting H₂O₂-induced MST1 activation *in vitro*, using purified PRX I and MST1 proteins. Collectively, my results show a novel PRX I function to cause cell death in response to high levels of oxidative stress by activating MST1, which underlies p53-dependent cytotoxicity caused by anticancer agents.

4.2. Introduction

Oxidative stress greatly affects diverse biological phenomena, including cell death, aging, and various disorders ranging from cancers to neurodegenerative diseases (1). However, molecular mechanisms by which oxidative stress is relayed inside cells remain poorly characterized. Protein kinases generally play key roles in signal transduction driven by various stimuli (53). For example, MST1 is a Ser/Thr kinase that is activated by apoptosis-inducing stimuli (54). Lehtinen *et al.* (55) reported that MST1 is activated by H₂O₂ and induces cell death by phosphorylating the transcription factor FOXO in primary mammalian neurons. Furthermore, Ste20 mediates H₂O₂-induced cell death by phosphorylating histone H2B in *S. cerevisiae* (56). These studies implicate MST1 as a crucial kinase in H₂O₂-induced cell death, but MST1 activation mechanisms by H₂O₂ have yet to be clarified.

MST1 is also known as a tumor-suppressor protein involved in death of cancer cells treated with anticancer drugs, such as cisplatin, a platinum-based DNA-damaging agent (57, 58). It is widely accepted that p53 is a key determinant for cell death in response to anticancer drugs (59, 60). By using *Drosophila* genetics, Colombani *et al.* (61) discovered that Dmp53 (*Drosophila melanogaster* p53) activates Hippo, the *Drosophila* MST1 homologue, to induce cell-death responses elicited by DNA-damaging ionizing radiation, suggesting a functional link between p53 and MST1. Moreover, it has been reported that p53-dependent apoptosis occurs via increasing oxidative stress (62-64). Indeed, the expression of p53 induces generation of mitochondrial ROS, likely causing MST1 activation. However, the precise mechanisms of p53-induced cell death via oxidative stress remain unknown.

Recent studies have revealed a role for H₂O₂ as a signaling molecule under various physiological/pathological settings (3-5). Several studies have found many H₂O₂-responsive proteins, among which PRXs are the most extensively characterized (10). The main function of PRXs generally has been thought to be H₂O₂ removal by catalyzing H₂O₂ reduction to H₂O. However, Jang *et al.* (65) reported quite unexpectedly that high levels of H₂O₂ stimulate PRX I and PRX II to form homo-oligomers with chaperone-like activities. In addition, Tpx1, the yeast PRX I homologue, mediates H₂O₂-induced activation of the p38/JNK homologue Sty1, by forming a transient, intermolecular disulfide bonding (66). Therefore, PRX I is now regarded not only as a scavenger of H₂O₂ but also as an important intermediate activating H₂O₂-responsive signaling pathways.

Here, I investigated the possible PRX I involvement in H₂O₂- and cisplatin-induced MST1 activation and cell death. In response to H₂O₂, PRX I formed oligomers that specifically associated with MST1. Overexpression and knockdown analyses indicated an essential role of PRX I in MST1 activation by H₂O₂ in cells. Live cell imaging analyses clearly showed that cisplatin treatment induced massive H₂O₂ generation also resulting in the PRX I oligomer formation. This occurred in a p53-dependent manner because primary MEFs obtained from *p53*^{-/-} mice did not form PRX I oligomers. Moreover, *p53*^{-/-} MEFs and PRX I-knockdown cancer cells were unable to activate MST1 in response to cisplatin and resisted cell death. Further, I successfully reconstituted MST1 activation by H₂O₂ and PRX I *in vitro*, using purified recombinant proteins.

4.3. Results

4.3.1. Specific association of MST1 with oligomeric PRX I

H₂O₂ induces both MST1 activation and PRX I oligomerization, prompting me to speculate that MST1 may be activated by associating with oligomeric PRX I. I first checked whether PRX I forms oligomers as reported previously. I ectopically expressed PRX I (wild-type (WT) and three different Cys mutants, C51S, C173S, and C83S) in COS7 cells, which were subsequently stimulated with H₂O₂. Cells were then harvested and cell lysates were subjected to native PAGE without SDS or reducing agents. As shown in Figure 25, WT PRX I formed significant amounts of oligomers appearing as a ladder on stained gels. In contrast, C173S PRX I constitutively formed oligomers but C51S or C83S PRX I did not even in the presence of H₂O₂. These results agree with previous studies (65, 67).

Having confirmed PRX I oligomerization, I examined the possible PRX I interaction with MST1. PRX I (WT and the Cys mutants) and MST1 were co-expressed and cell lysates were subjected to co-immunoprecipitation. The results clearly indicated that MST1 associates with WT PRX I depending on H₂O₂ stimulation. However, MST1 associated constitutively with C173S PRX I (Figure 26A), correlating well with the oligomeric status of PRX I (Figure 25). There are six different genes encoding PRX isoforms in mammalian genomes; PRX II is also reported to form oligomers (65). Therefore, I also examined whether MST1 associates with PRX II, but observed no positive signal (Figure 26B), indicating that MST1 interacted specifically with PRX I only.

I then performed co-immunoprecipitation analyses against endogenous MST1/2

and PRX I proteins in U2OS cells, and confirmed that they form complexes *in vivo* when cells were treated with H₂O₂ (Figure 27A). To examine the direct interaction between these proteins, I expressed and purified GST-MST1 and PRX I recombinant proteins. The purified proteins were incubated in the presence of H₂O₂ or the reducing agent DTT and then subjected to pull-down assay using glutathione beads. The results indicated a clear positive signal in the presence of H₂O₂ (Figure 28B), indicating their direct interaction. I also confirmed that the recombinant PRX I formed oligomers *in vitro* similar to those in cells.

4.3.2. PRX I mediates H₂O₂-induced MST1 activation

Because H₂O₂ stimulation is known to activate MST1, I next investigated the possible importance of PRX I in MST1 activation. Firstly, I co-expressed MST1 with PRX I (WT and the Cys mutants) in COS7 cells and examined MST1 autophosphorylation, which reflects MST1 activation (68). As shown in Figure 29A, the expression of WT PRX I significantly augmented MST1 autophosphorylation. In addition, C173S PRX I, which constitutively associates with MST1 (Figure 26), strongly induced MST1 autophosphorylation even without H₂O₂ stimulation. I also examined the effect of PRX II and found that it did not stimulate MST1 autophosphorylation (Figure 28B). Therefore, there was a very clear correlation between MST1 autophosphorylation and interaction with oligomeric PRX I. JNK1 is also known to be activated by H₂O₂ and play a crucial role in H₂O₂-induced signaling (69). Therefore, I examined the possible effect of PRX I expression on JNK1 activity. In contrast to the case of MST1, I did not observe any stimulatory effect of PRX I, although H₂O₂-induced activation of JNK1 was clearly observed (Figure 29).

As mentioned above, MST1 autophosphorylation is a useful marker for estimating MST1 activation, but whether MST1 kinase activity was actually promoted was still unknown. Therefore, I aimed to measure MST1 kinase activity directly by collecting MST1 protein by immunoprecipitation and performing kinase assays *in vitro*. Firstly, I used myelin basic protein as a substrate for assaying MST1 kinase activity, but found only a weak signal (data not shown). Therefore, I used GST-fusion MOBKL1B protein, which was reported to be a good MST1 substrate (70). I basically found similar results to those by the autophosphorylation analyses (Figure 30). Therefore, I confirmed MST1 activation by PRX I. Because MST1 activation has been linked to apoptosis, I next examined the effect of MST1 co-expression with PRX I on apoptosis as a biological measure for MST1 activation. When MST1 was ectopically expressed alone in U2OS cells, ~15% of cells underwent apoptosis showing typical chromatin condensation (Figure 31). A slight but significant increase in the apoptotic rate was observed by co-expression of WT PRX I, while C173S PRX I further enhanced the apoptotic rate to ~35%, which is consistent with the stronger ability of C173S PRX I to activate MST1 (Figure 28A and 30).

To examine the requirement of endogenous PRX I for H₂O₂-induced activation of endogenous MST1/2, siRNA against PRX I was introduced into U2OS cells to reduce endogenous PRX I expression. As shown in Figure 32A, treatment with PRX I siRNA specifically suppressed the expression of PRX I, without any significant effects on the PRX II expression. Cells were then stimulated with H₂O₂ and MST1/2 autophosphorylation was examined by immunoblotting. As shown in Figure 32B, H₂O₂ stimulation resulted in significant activation of endogenous MST1/2 in control cells, but it was clearly suppressed in PRX I-knockdown cells. Collectively, these results clearly

indicate that PRX I is an essential intermediate linking H₂O₂ stimulation to MST1 activation.

4.3.3. Cisplatin induces PRX I oligomer formation via p53

It has been reported that MST1 is important for anticancer drugs to induce cell death (58), prompting me to examine the possible roles of H₂O₂ and PRX I in this process. To confirm H₂O₂-generation, I performed H₂O₂-imaging analysis using GFP-HyPer, which specifically responds to H₂O₂ by increasing its fluorescent signal intensity (37). As shown in Figure 33, treatment of COS7 cells with cisplatin gradually increased the GFP-HyPer signal, which was evident after 4 hours. In contrast, I did not observe any significant increase in GFP-HyPer-expressing cells not treated with cisplatin or control GFP-expressing cells treated with cisplatin. Having confirmed the H₂O₂-generation, I next examined PRX I oligomer formation and found that cisplatin treatment could induce oligomers of both ectopically expressed PRX I in COS7 cells and endogenous PRX I in U2OS cells (Figure 34, A and B).

I noticed that p53 levels significantly increased in U2OS cells by cisplatin treatment (Figure 34B) as reported previously (71). Therefore, I next examined whether p53 plays any important role in PRX I oligomer formation induced by cisplatin treatment. As shown in Figure 35A, p53 ectopic expression by itself could induce PRX I oligomerization, which was abrogated by the antioxidant NAC treatment. I also examined the apoptotic rate of the cells and found that p53 expression raised the number of apoptotic cells with condensed chromatin (from 4.3% in control cells to 22.6% in p53-expressing cells, Figure 35B). This cell death was again inhibited by NAC treatment, and thus, PRX I oligomer formation correlated well with p53

apoptosis-inducing ability, suggesting a functional link between p53 and PRX I.

To indicate definite endogenous p53 requirement for cisplatin-induced H₂O₂-generation and PRX I oligomerization, I isolated MEFs from wild-type (*p53*^{+/+}) or p53-knockout (*p53*^{-/-}) mice and examined H₂O₂-generation and endogenous PRX I oligomer formation. The results clearly demonstrated that cisplatin treatment could induce H₂O₂-generation and PRX I oligomer formation in *p53*^{+/+} MEFs, but not in *p53*^{-/-} MEFs (Figure 36 and 37A). I further investigated the possible relationships with human cancers, which often lack functional p53, by performing similar experiments using human cancer-derived cell lines, such as U2OS (osteosarcoma, p53-positive), SaOS-2 (osteosarcoma, p53-negative), MCF-7 (breast cancer, p53-positive), and MDA-MB-231 (breast cancer, p53-mutated). As shown in Figure 37B, we could confirm that cisplatin-induced PRX I oligomer formation occurred in U2OS and MCF-7 cells but not in SaOS-2 and MDA-MB-231 cells, which is consistent with the functional status of p53.

4.3.4. PRX I mediates cisplatin-induced MST1 activation and cell death

It has been reported that cisplatin treatment induces MST1 activation (58). The results shown in Figure 34 to 37 clearly demonstrate that cisplatin induces PRX I oligomer formation via p53. Therefore, I speculated that PRX I may mediate cisplatin-induced MST1 activation. To test this hypothesis, I first examined the complex formation status by ectopically expressing MST1 and PRX I in COS7 cells and confirmed that cisplatin treatment significantly augmented the co-immunoprecipitation of the two proteins (Figure 38A). I next examined complex formation between endogenous MST1 and PRX I in U2OS cells. When cells were not treated with cisplatin,

only very weak co-immunoprecipitation signal was observed, but cisplatin treatment significantly increased this signal (Figure 38B).

To directly examine the importance of PRX I in cisplatin-induced MST1 activation, I next performed PRX I-knockdown analysis and found that MST1 activation was severely impaired in cells treated with PRX I siRNA (Figure 39A). I also examined the PRX I-knockdown effect on the apoptotic rate. I observed a slight increase in the apoptotic rate by PRX I-knockdown itself (4.7% in control cells to 12.3% in PRX-I-knockdown cells, Figure 39B). Because PRX I plays an important role in scavenging H₂O₂, this increase is probably caused by augmented oxidative stress. Cisplatin treatment induced a significant increase in the apoptotic rate in control cells (Figure 39B). However, PRX I-knockdown cells relatively resisted against cisplatin and their apoptotic rate was significantly lower than in control cells, thus revealing an unexpected role for PRX I in cell-death responses induced by cisplatin treatment. I also examined the importance of p53 in cisplatin-induced MST1 activation. MEFs obtained from *p53*^{+/+} or *p53*^{-/-} mice were treated with cisplatin and subsequently, levels of phosphorylated endogenous MST1/2 were examined by immunoblotting. As shown in Figure 40A, cisplatin-induced phosphorylation of MST1/2 was very weak in *p53*^{-/-} MEFs, which is consistent with the p53-dependent PRX I oligomer formation (Figure 37A). I also performed similar experiments by using human cancer cells and confirmed that p53-positive U2OS and MCF-7 cells activated MST1/2 in response to cisplatin, but SaOS-2 (p53-negative) and MDA-MB-231 (p53-mutated) cells did not (Figure 40B).

4.3.5. Mechanism of MST1 activation by PRX I and H₂O₂

Finally, I tried to clarify the molecular mechanisms of MST1 activation by PRX I

and H₂O₂. For this purpose, I purified various preparations of recombinant MST1 and PRX I proteins (Figure 41). I first incubated full-length MST1 with or without PRX I under reducing (10 mM DTT) or oxidizing (10 μM H₂O₂) condition, and then examined MST1 autophosphorylation. As shown in Figure 42A, levels of phosphorylated MST1 specifically increased when PRX I was with H₂O₂. Moreover, the results of kinase assays using MOBKL1B as a substrate also confirmed MST1 activation by PRX I and H₂O₂ (Figure 42B). Therefore, I successfully reconstituted H₂O₂-induced MST1 activation by PRX I, indicating a crucial role for PRX I in MST1 activation.

I then further explored molecular mechanisms underlying this activation. The *N*-terminal half of MST1 contains a kinase domain with the autophosphorylation site and the *C*-terminus includes an inhibitory domain for the kinase activity (68, 72). Thus, I created two GST-fusion MST1 fragments, lacking either the NH₂- or *C*-terminal region (GST-MST1 C or GST-MST1 N respectively) (Figure 41), and examined their binding ability to recombinant PRX I by pull-down assays. As shown in Figure 43A, GST-MST1 C, but not GST-MST1 N, could specifically precipitate PRX I in the presence of H₂O₂. Since MST1 N has been shown to possess increased kinase activity compared with full-length MST1 in similar kinase assays *in vitro* (72), I assumed that the direct interaction of the *C*-terminal region with the *N*-terminal kinase domain inhibits the kinase activity and that H₂O₂-induced association with PRX I abrogates this interaction, resulting in the opening of the kinase domain. Indeed, the interaction of recombinant MST1 C with GST-MST1 N was confirmed. Furthermore, this interaction was significantly weakened by addition of PRX I with H₂O₂, but not with DTT (Figure 43B). I next assessed the direct effect on the kinase activity by examining MST1 N autophosphorylation. Expectedly, MST1 C addition clearly reduced MST1 N

autophosphorylation (Figure 44), further supporting the above-mentioned regulatory mechanism. When I added PRX I to the mixture of MST1 N and MST1 C, PRX I could clearly negate autophosphorylation suppression induced by MST1 C only when incubation was under H₂O₂-driven oxidative condition. Based on these results, I concluded that oligomeric PRX I activates MST1 by dissociating the inhibitory C-terminal region of MST1 from the N-terminal kinase domain, thus mediating the H₂O₂-induced MST1 activation.

4.4. Discussion

Here I showed a quite unexpected MST1 activation mechanism by H₂O₂, mediated by oligomeric PRX I. I elucidated novel PRX I functions in signal transduction promoting appropriate responses to oxidative stress. I also demonstrated the important role of PRX I in p53-dependent cell death triggered by anticancer drug cisplatin. Recent studies have suggested a potential approach to treat cancers by manipulating their redox environment. In these studies, it has been indicated that cancer cells are very sensitive to artificial ROS elevation because most cancer cells are chronically subjected to oxidative stress and an additional increase in ROS levels brings the level of oxidative stress to a fatal degree (reviewed by Trachootham *et al.* (73)). For example, PEITC, a natural compound that promotes ROS generation, is reported to induce apoptosis selectively in cancer cells (74). Although cell death was attributed to aberrant regulation of H-Ras, JNK, and NF-κB, PRX-I-mediated MST1 activation probably also takes part in this process and further examinations of these pathways could facilitate development of better chemotherapeutic agents.

Recent studies have indicated the importance of a mammalian signaling pathway equivalent to the *Drosophila* Hippo pathway in tumor suppression (75, 76). In *Drosophila*, Hippo activates Warts (LATS1/2 in mammals) together with Salvador (WW45 in mammals). Activated Warts then excludes an oncogenic transcription factor Yorkie (YAP in mammals) from the nucleus and induces apoptosis. The Hippo pathway appears to be conserved in mammals, and the human genes for several pathway components have been found to be mutated in cancers (57, 75, 76). PRX I is also suggested to suppress cancer development because mice lacking the *PRXI* gene have a

short life span owing to frequent development of several cancers (77-79). In these reports, oncogenesis has been attributed to loss of PRX I peroxidase activity. However, mice lacking the *PRX II* gene, the closest homologue of *PRX I*, do not show cancers in any cell type or tissue (67, 80). PRX II is expressed in a wide variety of tissues and has a more potent peroxidase activity than PRX I (10, 67). Indeed, *PRX II*^{-/-} mice exhibit a massive increase in cellular ROS levels (80). Therefore, loss of peroxidase activity alone does not account for the cancer-forming phenotype in *PRX I*^{-/-} mice. It should be noted that PRX I, but not PRX II, is able to bind and activate MST1 (Figure 26B and 27B), which may explain the phenotypic differences between *PRX I*^{-/-} and *PRX II*^{-/-} mice.

PRX I and PRX II are highly homologous proteins (91% homology and 78% identity in human) and thus expected to play similar roles intracellularly. However, my study clearly shows a difference in their role related to MST1 (Figure 26B and 28B). One possible reason may be in their oligomerization tendency because PRX I promptly forms oligomers in response to low H₂O₂ levels, whereas PRX II is comparatively resistant to H₂O₂-induced oligomerization (67). This difference can be attributed to the presence of PRX I Cys83, which is absent in PRX II. PRX I Cys83 reportedly forms a disulfide linkage with another PRX I Cys83, thus promoting homo-oligomer formation. Consistently, my study also confirmed that C83S PRX I did not efficiently form oligomers (Figure 25), only weakly binding and activating MST1 (Figure 26A and 27A).

PRX I is a well-known antioxidant enzyme thought to protect cells against oxidative stress by reducing H₂O₂ (10). Indeed, there are several reports indicating that PRX I inactivation results in elevation of ROS levels and oxidative DNA damage (9,

77-79). However, I demonstrated here a quite unexpected PRX I function, linking ROS to cell death. This difference in PRX I function apparently depends on the degree of oxidative stress. PRX I reduces H_2O_2 and protects cells from oxidative stress when H_2O_2 level is within a manageable range. However, when cells are exposed to excessive H_2O_2 levels, PRX I is inactivated as a peroxidase and forms oligomers (65, 81), thus resulting in MST1 activation. In this case, I postulate that PRX I contributes to protection of the whole organism by removing cells severely damaged by excess ROS, avoiding cancer development.

4.5. Figures

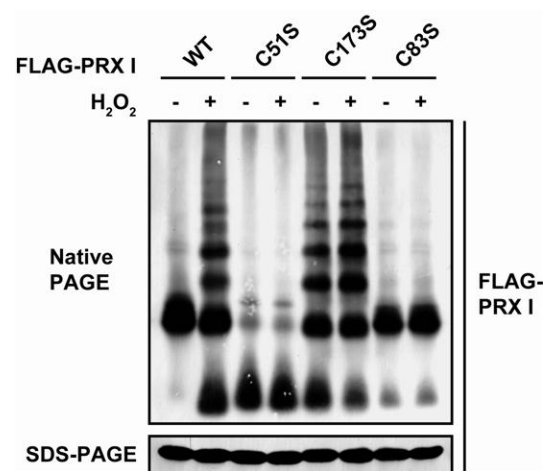


Figure 25. H₂O₂-induced oligomer formation of PRX I.

COS-7 cells were transfected with the indicated constructs and treated with 100 μ M H₂O₂ for 30 min. Cell lysates were treated with IAA and immunoblotted under native (without SDS or reducing agents) or denaturing (with SDS and reducing agents) conditions.

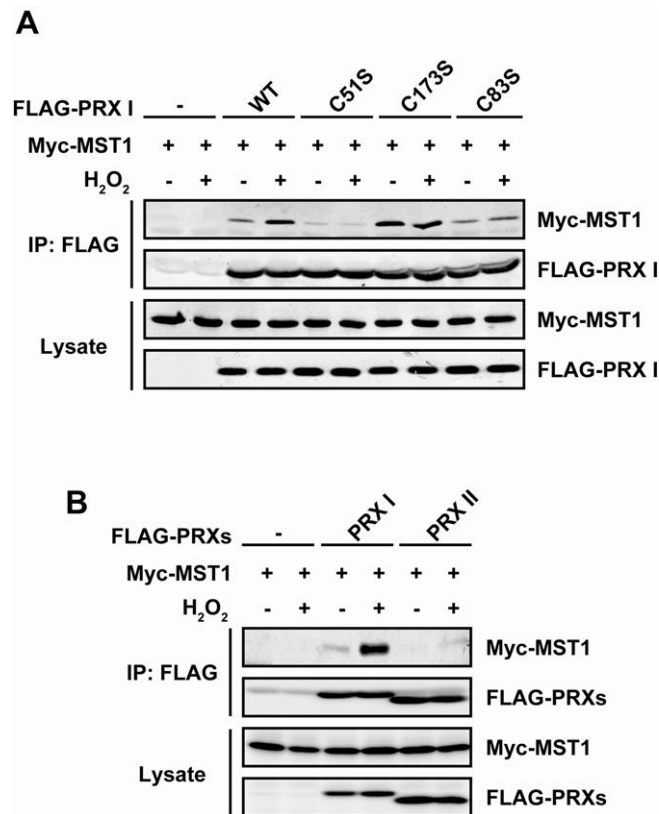


Figure 26. Specific association of MST1 with oligomeric PRX I.

(**A** and **B**) COS-7 cells were transfected with the indicated constructs and treated with 100 μ M H₂O₂ for 30 min. Cell lysates were immunoprecipitated (IP) with an anti-FLAG antibody and analyzed by immunoblotting using indicated primary antibodies.

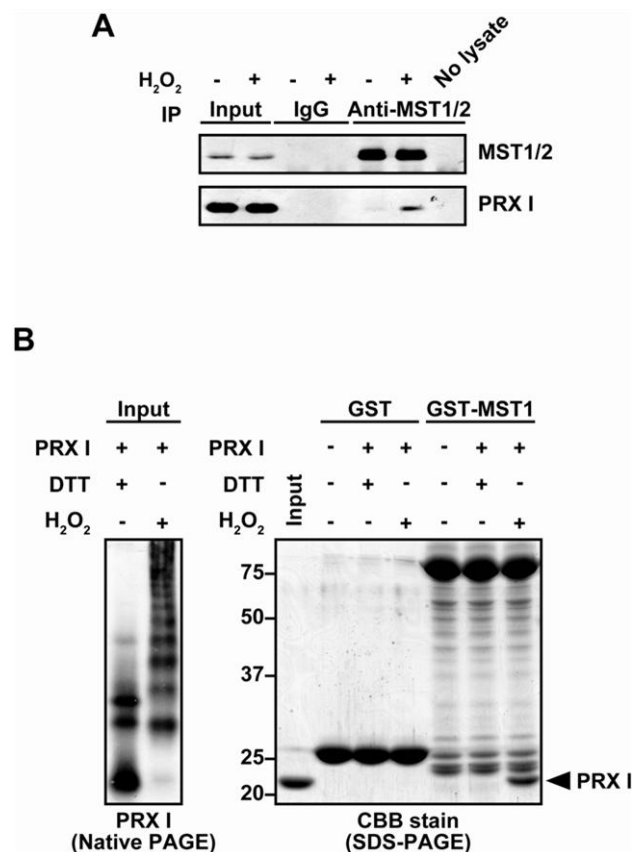


Figure 27. Association of MST1 with PRX I *in vitro* and *in vivo*.

(A) Lysates of U2OS osteosarcoma cells treated with 500 μ M H₂O₂ for 30 min were immunoprecipitated with anti-MST1/2 antibodies and immunoblotted with indicated primary antibodies.

(B) GST-MST1 pull-down assays of recombinant PRX I in the presence of 10 mM DTT or 10 μ M H₂O₂. Proteins were subjected to SDS-PAGE and Coomassie Brilliant Blue (CBB)-staining. Immunoblot of recombinant PRX I subjected to native PAGE is also given (left).

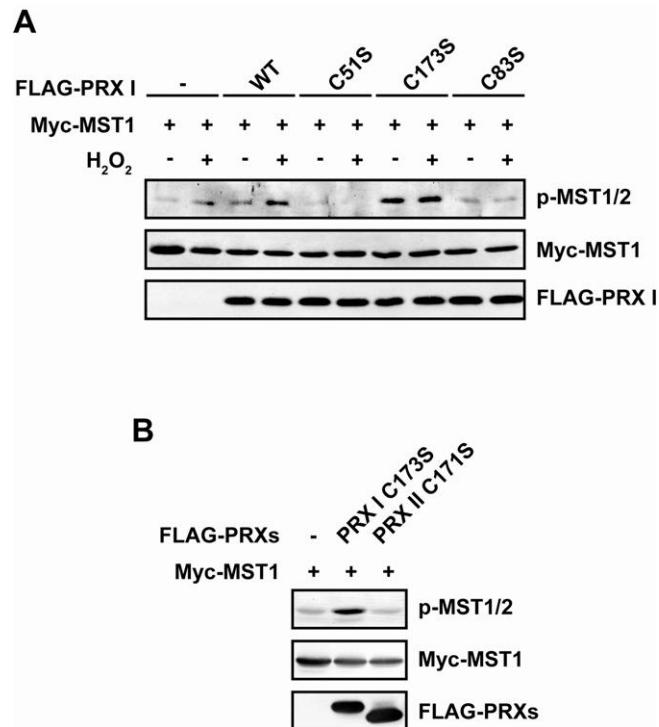


Figure 28. PRX I mediates H₂O₂-induced MST1 autophosphorylation.

(**A** and **B**) COS-7 cells were transfected with the indicated constructs and treated with 100 μ M H₂O₂ for 30 min. Cell lysates were analyzed by immunoblotting with indicated primary antibodies.

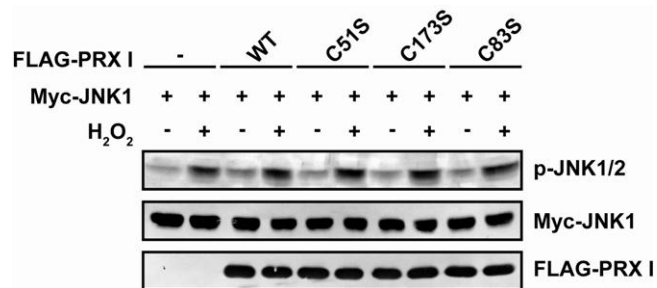


Figure 29. PRX I does not stimulate H₂O₂-induced JNK1 phosphorylation.

COS-7 cells were transfected with the indicated constructs and treated with 100 μ M H₂O₂ for 30 min. Cell lysates were analyzed by immunoblotting with indicated primary antibodies.

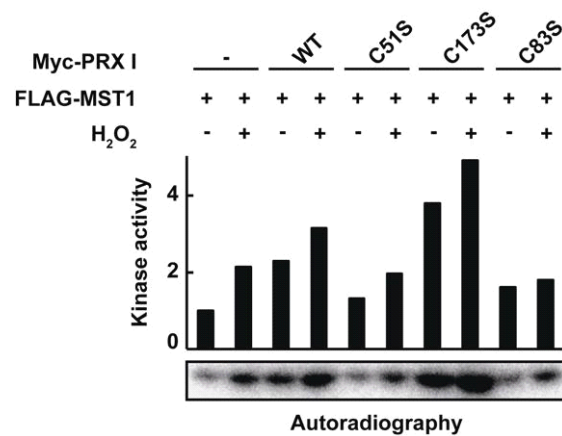


Figure 30. PRX I mediates H₂O₂-induced MST1 activation.

COS-7 cells were transfected with the indicated constructs and treated with 100 μ M H₂O₂ for 30 min. Cell lysates were immunoprecipitated with an anti-FLAG antibody and subjected to *in vitro* kinase assays using [γ -³²P]ATP and recombinant MOBKL1B as the substrate. The phosphorylation level of MOBKL1B was analyzed by autoradiography and the relative radioactivity is indicated.

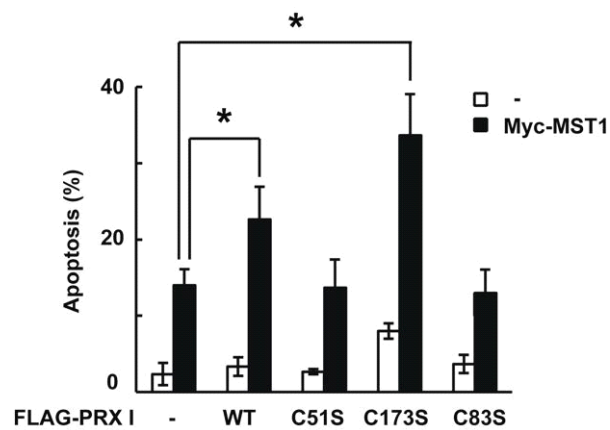


Figure 31. The effect of MST1 co-expression with PRX I on apoptosis.

U2OS cells were transfected with the indicated constructs together with GFP-expressing plasmids. They were fixed and DAPI-stained to visualize chromatin condensation. GFP-positive cells were examined for apoptosis. Data are mean \pm SEM for $n = 3$. For each experiment, more than 100 cells were examined. $*p < 0.05$ indicates the significant difference by one-way analysis of variance ($p = 0.004$) followed by Dunnett's multiple comparison test among the Myc-MST1 transfected groups.

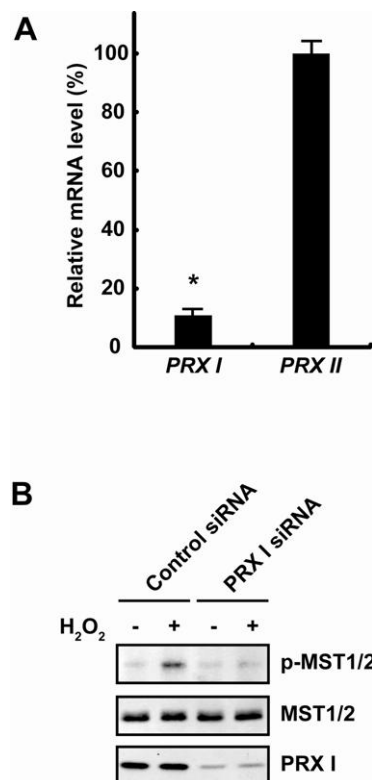


Figure 32. PRX I is necessary for H₂O₂-induced MST1 antophosphorylation.

(A) U2OS cells were transfected with siRNA against PRX I, and the relative mRNA levels of PRX I and PRX II (against control siRNA transfectants) were analyzed by real time PCR analyses. Data are mean \pm SEM for $n = 3$. * $p < 0.05$ indicates statistical significance by the Student's t test.

(B) U2OS cells were transfected with PRX I siRNA and treated with 100 μ M H₂O₂ for 30 min. Cell lysates were analyzed with indicated primary antibodies.

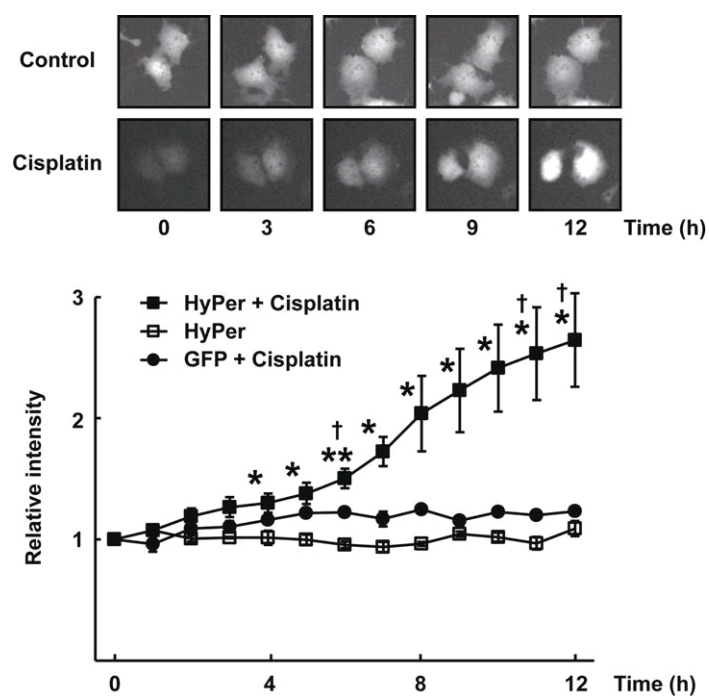


Figure 33. Cisplatin induces H₂O₂ production.

COS-7 cells were transfected with GFP-HyPer-expressing plasmids and then treated with 25 μ M cisplatin for indicated durations. Relative intensity of the GFP-fluorescence in cells was analyzed. Data are mean \pm SEM for $n = 3$. For each experiment, more than 50 cells were examined. * $p < 0.05$, ** $p < 0.01$ (against the “HyPer” group) and † $p < 0.05$ (against the “GFP + Cisplatin” group) indicate the significant difference by one-way analysis of variance ($p < 0.05$) followed by Bonferroni's multiple comparison test.

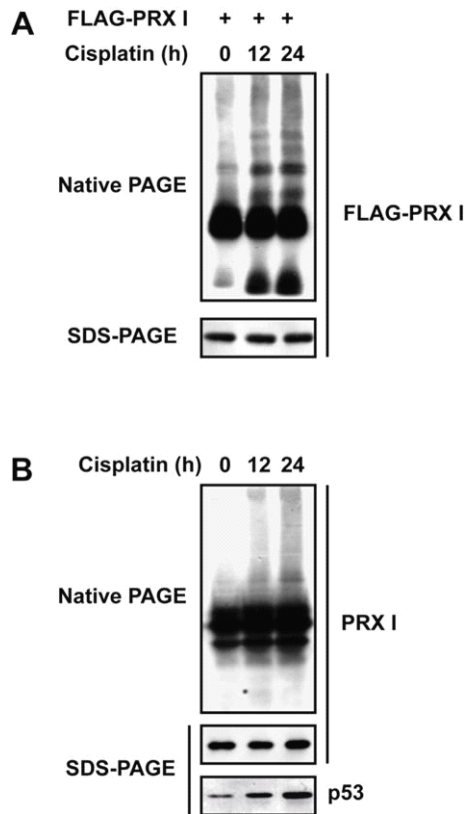


Figure 34. Cisplatin induces oligomer formation of PRX I.

(**A**) COS-7 cells transfected with the indicated constructs were treated with cisplatin for indicated durations. Cell lysates were treated with IAA and immunoblotted under native or denaturing conditions.

(**B**) U2OS cells were treated with cisplatin for indicated durations. Cell lysates were treated with IAA and immunoblotted under native or denaturing conditions.

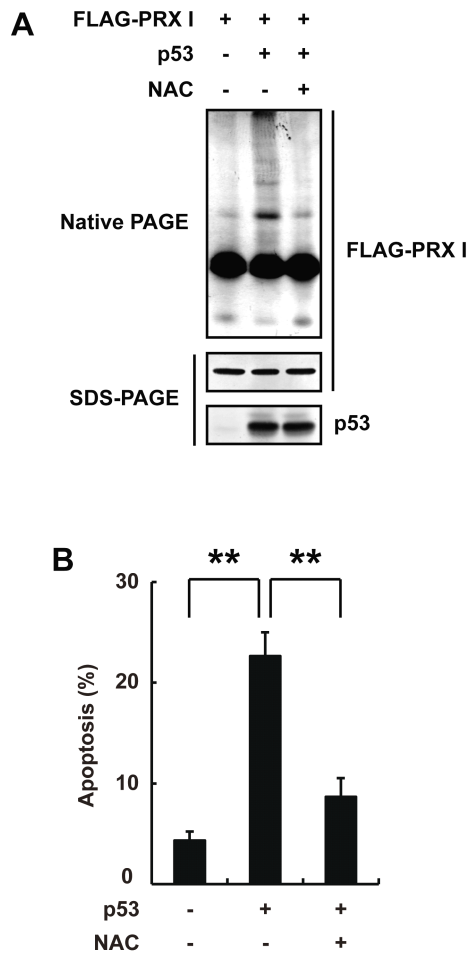


Figure 35. p53 induces oligomer formation of PRX I.

(A) U2OS cells were transfected with the indicated constructs and treated with NAC. Cell lysates were treated with IAA and immunoblotted under native or denaturing conditions.

(B) U2OS cells were transfected with the indicated constructs together with GFP-expressing plasmids and treated with NAC. Cells were fixed and DAPI-stained to visualize chromatin condensation. GFP-positive cells were examined for apoptosis. Data are mean \pm SEM for $n = 3$. For each experiment, more than 100 cells were examined. $**p < 0.01$ indicates significant difference by one-way analysis of variance ($p = 0.0009$) followed by Bonferroni's multiple comparison test.

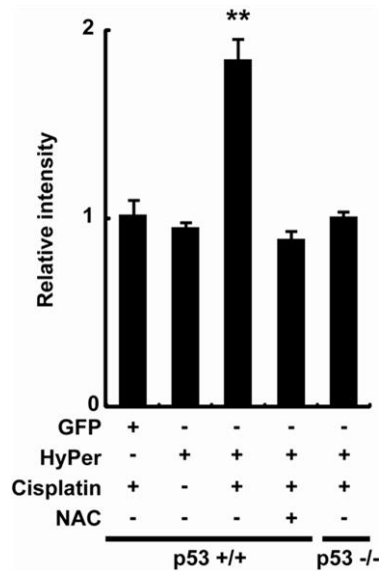


Figure 36. Cisplatin induces H₂O₂-generation via p53.

MEFs from p53^{+/+} or p53^{-/-} mice were transfected with the indicated constructs, and then treated with cisplatin for 12h. Relative intensity (compared to the initial time point) of the GFP-fluorescence in cells was analyzed. Data are mean \pm SEM for n = 3. For each experiment, more than 50 cells were examined. **p < 0.01 indicates significant difference by one-way analysis of variance (p = 0.0003) followed by Bonferroni's multiple comparison test.

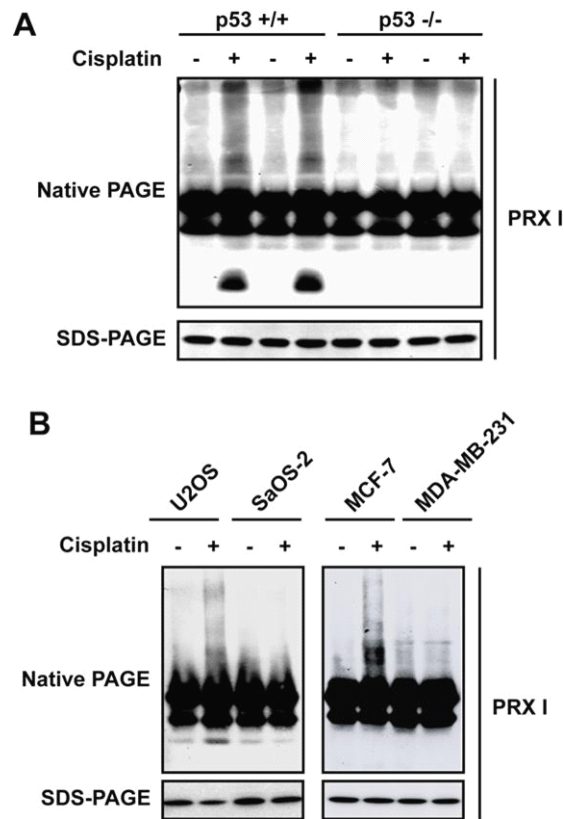


Figure 37. Cisplatin induces oligomer formation of PRX I via p53.

(A) MEFs from $p53^{+/+}$ or $p53^{-/-}$ mice were treated with cisplatin. Cell lysates were treated with IAA and immunoblotted under native or denaturing conditions.

(B) human cancer-derived cell lines such as U2OS, SaOS-2, MCF-7, and MDA-MB-231 were treated with cisplatin. Cell lysates were treated with IAA and immunoblotted under native or denaturing conditions.

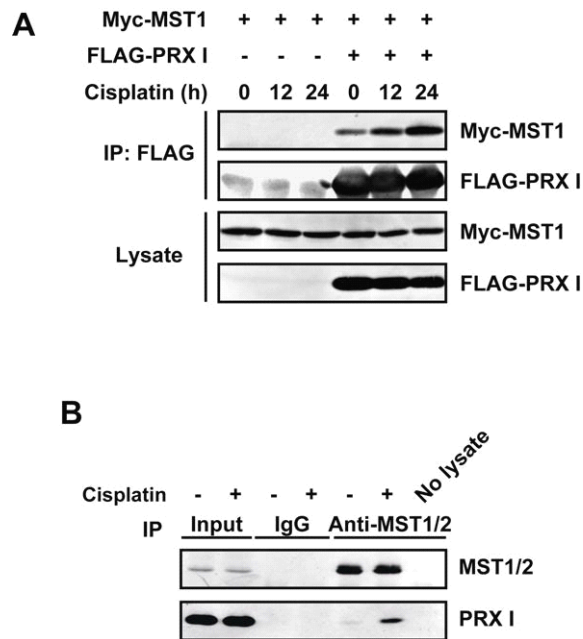


Figure 38. Cisplatin promotes PRX I-MST1 interaction.

(A) COS-7 cells were transfected with the indicated constructs and treated with cisplatin for indicated durations. Cell lysates were immunoprecipitated with anti-FLAG antibodies and analyzed by immunoblotting using indicated primary antibodies.

(B) Lysates of U2OS cells treated with cisplatin were immunoprecipitated with anti-MST1/2 antibodies and immunoblotted with indicated primary antibodies.

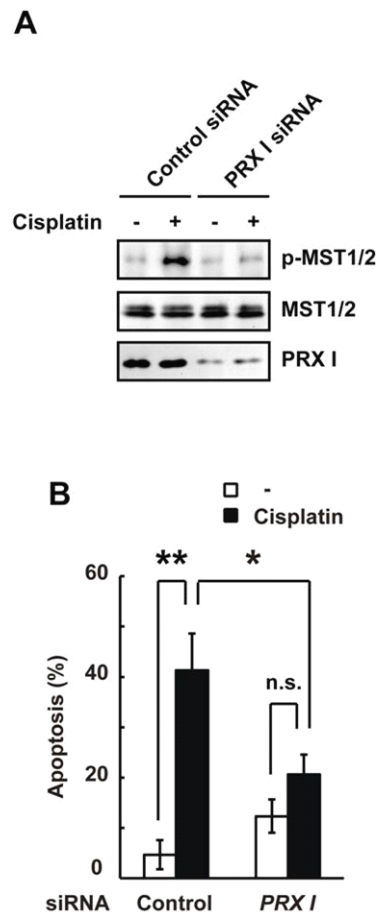


Figure 39. PRX I is necessary for cisplatin-induced MST1 activation.

(A) U2OS cells were transfected with PRX I siRNA and treated with cisplatin. Cell lysates were analyzed with indicated primary antibodies

(B) U2OS cells were transfected with PRX I siRNA together with GFP-expressing plasmids and treated with cisplatin. Cells were fixed and DAPI-stained to visualize chromatin condensation. Apoptosis was assessed in GFP-positive cells. Data are mean \pm SEM for $n = 3$. For each experiment, more than 100 cells were examined. * $p < 0.05$, ** $p < 0.01$ indicate significant difference by one-way analysis of variance ($p = 0.0029$) followed by Bonferroni's multiple comparison test.

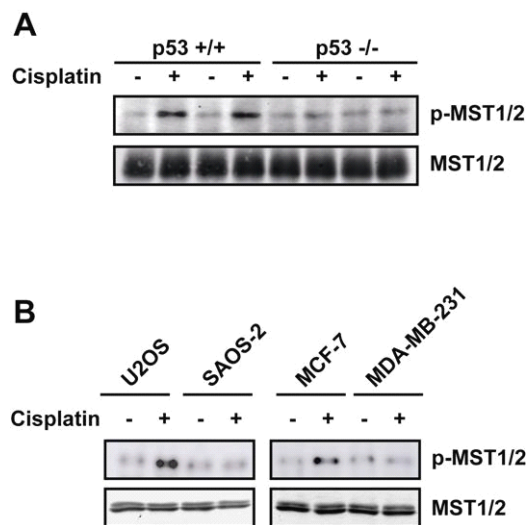


Figure 40. p53 is necessary for cisplatin-induced MST1 autophosphorylation.

(A) MEFs from $p53^{+/+}$ or $p53^{-/-}$ mice were treated with cisplatin. Cell lysates were analyzed with indicated primary antibodies.

(B) human cancer-derived cell lines such as U2OS, SaOS-2, MCF-7, and MDA-MB-231 were treated with cisplatin. Cell lysates were analyzed with indicated primary antibodies.

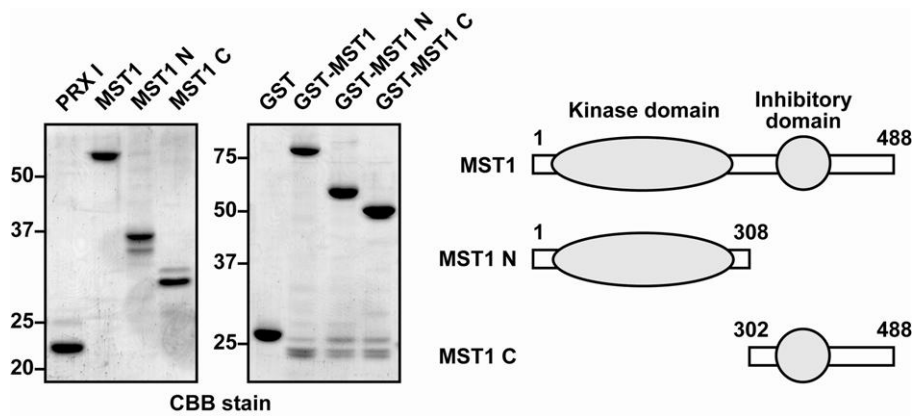


Figure 41. Expression and purification of recombinant proteins of PRX I and MST1.

Purified recombinant proteins expressed in *E. coli* or Sf9 cells were analyzed by SDS-PAGE and CBB-staining. Schematics illustrate MST1 constructs.

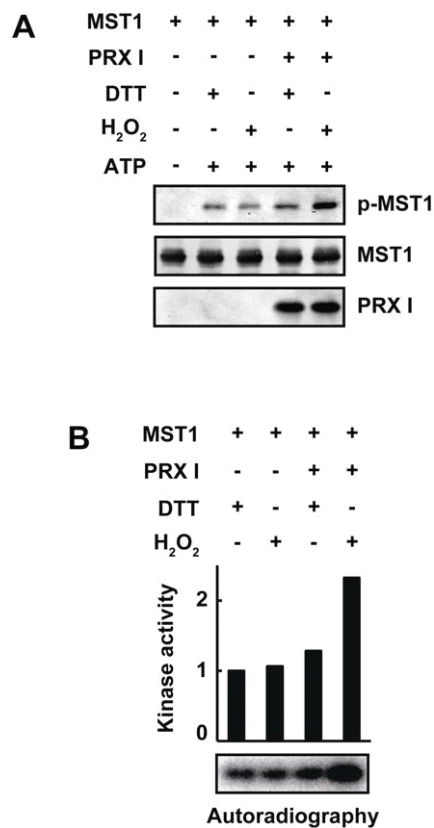


Figure 42. *In vitro* reconstitution of H₂O₂-induced MST1 activation by PRX I.

(**A**) *In vitro* kinase assays were performed by mixing indicated recombinant proteins in the presence of 10 mM DTT or 10 μ M H₂O₂. Proteins were analyzed using indicated primary antibodies.

(**B**) *In vitro* kinase assays using [γ -³²P]ATP were performed using indicated recombinant proteins and recombinant MOBKL1B as substrates in the presence of 10 mM DTT or 10 μ M H₂O₂. Phosphorylation of MOBKL1B was analyzed by autoradiography and the relative radioactivity is indicated.

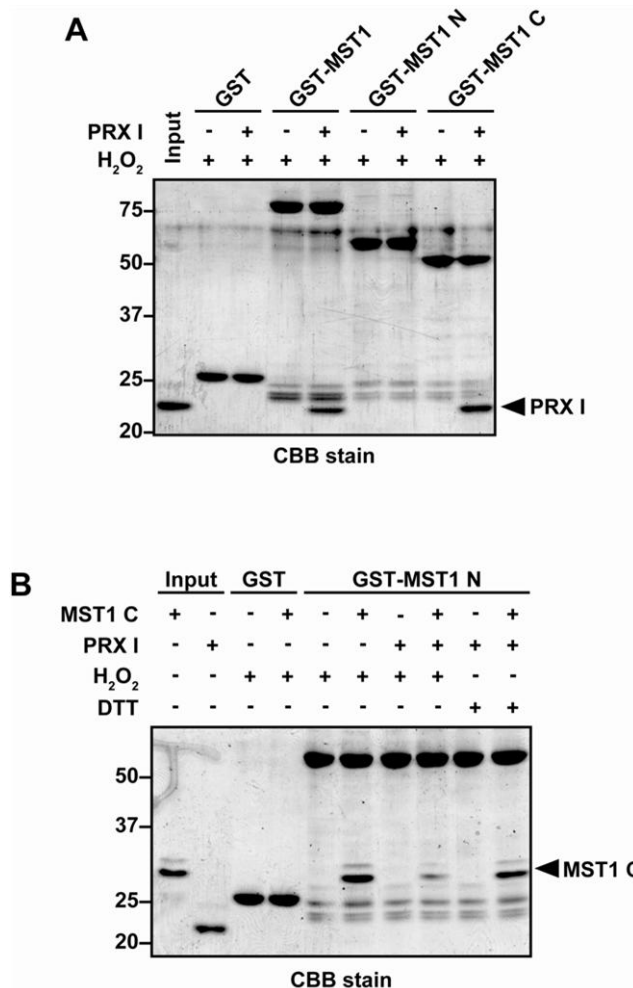


Figure 43. MST1 interacts with PRX I through *C* terminus domain.

(A) GST-MST1 pull-down assays for PRX I. Proteins were subjected to SDS-PAGE and CBB-staining.

(B) GST-MST1 pull-down assays for MST1 C in the presence of PRX I. Proteins were subjected to SDS-PAGE and CBB-staining.

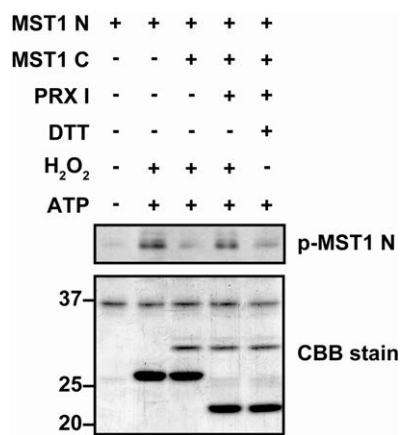


Figure 44. MST1 is activated by PRX I through *C* terminus domain.

In vitro kinase assays were performed using indicated recombinant proteins in the presence of 10 μ M H₂O₂ or 10 mM DTT. Proteins were analyzed with indicated primary antibodies or CBB-staining.

5. Materials and Methods

5.1. Antibodies and reagents

The following commercially available antibodies were used: rabbit anti-TRX (Chemicon and Redox Bio Science); mouse anti-CRMP2 (Immuno-Biological Laboratories); rabbit anti-Akt, rabbit anti-phospho-Akt (Ser473), rabbit anti-phospho-GSK3 α/β (Ser21/9), rabbit anti-phospho-MST1/2 (Thr183), rabbit anti-JNK1/2, rabbit anti-phospho-JNK1/2 (Thr183/Tyr185) (Cell Signaling Technology); mouse anti-GSK3 β (BD Transduction Laboratories); mouse anti-FLAG (M2), mouse anti- β -tubulin (Sigma); rabbit anti-Myc (A-14), mouse anti-Myc (9E10), rabbit anti-Slp1, rabbit anti-DHC (Santa Cruz Biotechnology); mouse anti- β -actin (Chemicon); rabbit anti-Numb, rabbit anti-PRX I (Abcam); rabbit anti-MST1/2 (Bethyl Laboratories); mouse anti-p53 (Ab-6) (Calbiochem).

The rabbit antibody against CRMP2 was generated by immunizing rabbits with recombinant His-CRMP2 as an antigen and following affinity purification with GST-CRMP2. New Zealand white rabbits were immunized with recombinant His-CRMP2 (amino acids 404-572) together with complete Freund's adjuvant every 2 weeks for 5 times. 2 weeks after fifth immunization, blood was gathered from rabbits and serum was separated. Serum was incubated with GST-CRMP2-conjugated agarose beads for over night at 4 °C. The beads were then washed 5 times with lysis buffer (20 mM Tris-HCl (pH 7.5), 150 mM NaCl, 5 mM EDTA, 0.5% Triton X-100) and the bound antibody was extracted from beads with glycine buffer (100 mM Glycine-HCl (pH 3.0)) and rapidly diluted with PBS. Specificity of the antibody against CRMP2 and TRX are indicated in Figure 24. Rabbit anti-phospho-CRMP2 (p-CRMP2) antibody that

recognizes phosphorylated Thr514 and rabbit anti-KLC1 were as previously described (19, 39).

DNCB, NAC, NADPH and purified TxR protein (Sigma) and cisplatin (Yakult Honsha) were from commercial sources.

5.2. Plasmid constructs and siRNA

The human GSK3 β and mouse NRX cDNAs were obtained as previously described (82, 83). The human CRMP2 cDNA was obtained from I.M.A.G.E clones (clone ID 6177866; Invitrogen). The cDNAs for mouse TRX, human TRP14, human TRP32, mouse CDK5, mouse p25, mouse PRX I, mouse PRX II, human MST1, human JNK1, and human MOBKL1B were generated by RT-PCR. cDNAs were amplified by PCR and inserted into pDrive plasmid vectors. PCR was performed under the following program: 95 °C for 30 sec; 95 °C for 30 seconds, 60 °C for 30 seconds and 72 °C for 1 minute / 1000 bp DNA, for 25 cycles; 4 °C for 10 minutes. The mouse MICAL1 cDNA was kindly provided by Kazusa DNA Research Institute (clone name msh04044). The GFP-HyPer cDNA was purchased from Evrogen.

Site-directed mutagenesis was conducted using the Quick-Change Mutagenesis Kit (Stratagene). Primers were designed to be 25 bp duplex enclosing the mutated bases. PCR was performed under the following program: 95 °C for 30 sec; 95 °C for 30 seconds, 60 °C for 30 seconds and 72 °C for 1 minute / 1000 bp of DNA, for 18 cycles; 4 °C for 10 minutes. To construct TRX Rsc, T at position 73, T at position 76 and C at position 79 in the open reading frame of mouse TRX were replaced to G, G, and A, respectively. To construct MICAL GW, three glycine residues at position 91, 93, and 96 of mouse MICAL1 protein were replaced to tryptophan residues. MST1 lacking

C-terminus (MST1 N, 1-308) and N-terminus (MST1 C, 302-488) were generated by PCR. The cDNA fragments were inserted into pEF-BOS, pCAGGS (Clontech Laboratories) for the expression in culture cells, pGEX-2T, pGEX-2T modified to generate proteins tagged with GST at the C-terminus, pGEX-6P1 (GE Healthcare), and pQE30 (Qiagen) plasmid vectors for the expression in *E. coli*. and pFastBac1 (Invitrogen) for the expression in Sf9 cells.

Sema3A fused to alkaline phosphatase or control alkaline phosphatase expression plasmid was as previously described (15). Myc-PlexA2 and NP-1 expression plasmids were as previously described (44).

The siRNA duplex oligonucleotides against rat TRX (#1, #2, and #3), rat MICAL1 and MICAL3, and human PRX I were purchased from Invitrogen. The control siRNA had the shuffled sequence of #1 siRNA and was designed as a non-silencing siRNA that does not correspond to any known mammalian mRNA sequence. The target mRNA sequences are: TRX#1, 5'-CCAATGTGGTGTTCCTTGAAGTAGA-3'; TRX#2, 5'-CCTCTGTGACAAGTATTCCAATGTG-3'; TRX#3, 5'-GAGTTCTCTGGTGCTAACAAGGAAA-3'; Control, 5'-GAGTCTCGTGGAATCGAACGTTAAA-3'; MICAL1, 5'-GGCAGAATATGAGTTGGGCATCATA-3'; MICAL3, 5'-CCCTGTCACTAGGTATCCCAATATT-3'; PRX I, 5'-ATGTTTGTGAGTGAAGTGAAGGCC-3'.

5.3. Recombinant proteins

Recombinant proteins of CRMP2, TRX, CDK5, p25, GSK3 β , MST1, PRX I, and MOBKL1B were expressed as GST fusions in *E. coli* (CRMP2, TRX, PRX I and

MOBKL1B) or in Sf9 cells (CDK5, p25, GSK3 β , MST1, MST1 N, and MST1 C). *E. coli* (BL20) transformed with pGEX-2T or pGEX-6p1 were precultured for overnight in LB media. The culture medium was diluted for 100 times, incubated for 3 hours at 37 °C and then stimulated with 0.5 mM IPTG for 4 hours at 20 °C. *E. coli* was precipitated, diluted with lysis buffer and sonicated. Sf9 cells were infected with baculovirus and cultured for 3 days in Sf-900 II medium (Invitrogen). Cells were precipitated, diluted with lysis buffer and sonicated. Baculovirus was created using Bac-to-Bac Baculovirus Expression System (Invitrogen). *E. coli* (DH10Bac) was transformed with pFastBac1 and bacmids were harvested. Sf9 cells were transfected with bacmids using oligofectamine (Invitrogen), cultured for 3 days and culture medium containing baculovirus was harvested.

These lysates were incubated with glutathione-sepharose beads (GE Healthcare) for 2 hours at 4 °C, washed with lysis buffer for 5 times and eluted with lysis buffer containing excess glutathione (300 mM). GST-tag was removed by incubating GST-fusion proteins bound to glutathione sepharose with thrombin (GE Healthcare) for proteins from pGEX-2T or PreScission protease (GE Healthcare) for proteins from pGEX-6P1 for 4 hours at 4 °C. Thrombin was removed by incubating proteins with benzamidine-sepharose beads (Sigma) for 4 hours at 4 °C.

5.4. Cell culture and transfection

COS-7, N1E-115, U2OS, SaOS-2, and *p53*^{+/+} or *p53*^{-/-} MEFs were cultured in DMEM with 10% FBS, and MCF-7 and MDA-MB-231 cells were cultured in RPMI1640 with 10% FBS, at 37 °C in 5 % CO₂. SaOS-2 and MCF-7 cells were obtained from Japanese Collection of Research Bioresources, and MDA-MB-231 cells

were from American Type Culture Collection. COS-7 and U2OS cells were generous gifts from Dr. Tadaomi Takenawa (Kobe University) and Kiyoko Fukami (Tokyo University of Pharmacy and Life Sciences), respectively. The cancer cells are routinely authenticated through cell morphology monitoring and growth curve analysis, and I confirmed that p53 status agrees with the information on the International Agency for Research on Cancer TP53 database (<http://www-p53.iarc.fr/>). Primary MEFs were derived from 13.5-day embryos and genotyped by PCR. *p53^{+/-}* mice were purchased from RIKEN BioResource Center (BRC) (84). *p53^{+/-}* embryos were derived from *p53^{+/-}* crosses maintained on a C57BL/6C background.

Cells were seeded in 36 or 60-mm dishes, cultured overnight, and transfected with Lipofectamine 2000 (Invitrogen). Plasmid DNA and Lipofectamine 2000 were mixed with OPTI-MEM respectively and incubated for 5 minutes. Then these were mixed, incubated for 20 minutes and applied to cells in antibiotic-free medium. 6 hours after transfection, medium was changed for those containing antibiotics. Cells were washed with PBS and harvested with lysis buffer 1 or 2 days after transfection.

5.5. Non-reducing SDS-PAGE, native PAGE and immunoblotting

Cell lysates in non-reducing SDS-PAGE sample buffer (50 mM Tris-HCl (pH 6.8), 10% glycerol, 1% SDS and 15 mM IAA) were incubated for 30 minutes at 37 °C with frequent mixing and subjected to non-reducing SDS-PAGE. In the case of DRG neurons, cells were cultured in medium with 15 mM NAC (Sigma) for 3 hours and then cultured in NAC-free medium. After 1 hour, cells were treated with H₂O₂ or stimulated with Sema3A for the indicated time and harvested. For native PAGE, cell lysates in native PAGE sample buffer (50 mM Tris-HCl (pH 6.8), 10% glycerol, 1% deoxycholate and

15 mM IAA) were subjected to native PAGE. All buffers and poly-acrylamide gels were free from SDS and the cathode buffer contained 1 % deoxycholate (85).

After PAGE, proteins in poly-acrylamide gels were transcribed into blotting membranes at 1 mA / 1 cm² for 2 hours. Membranes were blocked with blocking buffer (5 % skim milk, 5 % BSA in PBS) for 1 hour and incubated with primary antibodies for 1 hour and subsequently alkaline phosphatase-conjugated secondary antibodies for 30 minutes. Signals were visualized with NBT and BCIP (Sigma).

5.6. Identification of TRX target proteins

NIH-3T3 cell lines stably expressing FLAG-TRX C35S or C32/35S were created by transfecting pEF-BOS expressing these proteins together with hygromycin-resistant plasmid vectors and subsequently selecting hygromycin-resistant cells. The protein expression was evaluated by immunoblotting. For identification of TRX target proteins, lysates of NIH-3T3 cells stably expressing FLAG-TRX C35S or C32/35S were incubated with anti-FLAG M2 agarose beads (Sigma) for 2 hours at 4 °C. The beads were washed 5 times and then incubated with lysis buffer containing 5 mM DTT. The eluted proteins were separated by SDS-PAGE and stained with the Silver Quest silver staining kit (Invitrogen). The bands of interest were excised from the gel and treated with trypsin. The resulting peptides were purified and analyzed by MALDI/TOF-MS/MS (4700 Proteomics Analyzer; Applied Biosystems).

5.7. Preparation of rat DRG and growth cone collapse assays

DRG neurons were prepared as previously described (15, 17). DRG were removed from the E14 Sprague Dawley rats. DRG were incubated with 0.2 % trypsin for 10

minutes at 37 °C and dissociated with fire-polished pasteur pipettes. Dissociated neurons were then transfected with various expression plasmids together with GFP-expressing plasmid using the Nucleofector device with the rat neuron nucleofector kit and program O-03 (Lonza Group AG) and plated on glass slides coated with poly-D-lysine (Sigma) and laminin (BD Biosciences). DRG neurons were cultured for 16 hours in Ham's F12 medium with 10% FBS and 20 nM NGF, and then the medium was replaced with NGF-free one. Cells were cultured for an additional 3 hours and then stimulated with 0.5 nM Sema3A.

The Sema3A proteins were prepared as reported previously (17, 44). Briefly, HEK293 cells were transiently transfected with Sema3A-expressing plasmid with Lipofactamine 2000 Reagent (Invitrogen), and then the culture medium (conditioned medium) was collected after 48 hours, which was used for stimulating neurons in culture. The amount of Sema3A proteins in the conditioned medium was determined by quantitative immunoblotting analyses. After stimulation with Sema3A, neurons were fixed with 1 % formaldehyde and 10 % sucrose in PBS for 30 minutes and growth cones were visualized by staining with rhodamine-phalloidin for 30 minutes. GFP positive cells were measured for collapse response. For each experiment, more than 50 neurons were measured.

5.8. Preparation of chicken DRG and growth cone turning assays

Growth cone turning induced by an extracellular gradient of Sema3A was performed as described previously (34, 86). DRG neurons from embryonic day 9 chicks were dissociated and plated on a glass-based dish coated with poly-D-lysine and laminin for several hours. 10 μ M DNCB (Sigma) were bath-applied to culture medium

at least 60 min before the application of Sema3A gradients. To examine the function of CRMP2 C504S on growth cone turning, dissociated neurons were transfected with either Myc-CRMP2 WT or C504S-expressing plasmids together with GFP-expressing plasmid using the Nucleofector device and cultured overnight. The transfected cells were identified by GFP fluorescence. Sema3A gradients were applied with a micropipette containing Sema3A (100 µg/ml in pipette, R&D Systems). Micropipettes were set 100 µm from the growth cone at a 45° angle with respect to the original direction of axon elongation.

5.9. *In utero* electroporation and quantification of fluorescence intensities

Pregnant ICR mice were purchased from SLC Japan. *In utero* electroporation was performed as previously described (87, 88). Electroporated brains were cut into 16 µm coronal sections with a cryostat (Leica Microsystems). Fluorescence images of frozen sections of EGFP-expressing mouse brains were captured by TCS SL laser scanning confocal microscopy (Leica Microsystems). Fluorescence intensities inside similar width rectangles in various regions of the cerebral cortex (layers II-IV, V-VI, and IZ and VZ/SVZ) were measured by the TCS SL software as previously described (87). Relative intensities to the total fluorescence were calculated and plotted in the graphs with standard errors.

5.10. H₂O₂-imaging analyses

Imaging analyses were performed using an Olympus IX81 microscope equipped with an Olympus DP30BW camera. GFP-HyPer was excited at 480 nm and fluorescence from GHP-HyPer was monitored at 525 nm. DRG neurons were cultured

in glass base dishes (IWAKI) coated with Poly-D-lysine and laminin. Images were taken for every minute after Sema3A stimulation. U2OS cells were cultured in glass base dishes coated with Poly-D-lysine. Images were taken for every 15 minutes after cisplatin treatment. I quantified image intensities with DP Controller software (Olympus) and ImageJ software (National Institutes of Health, U.S.A.).

5.11. *In vitro* kinase assay

The kinase reaction was assessed in a kinase buffer (20 mM Tris-HCl (pH 7.5), 15 mM MgCl₂) containing either 10 mM DTT or 10 μM H₂O₂. Recombinant CRMP2 or MOBKL1B was used as the substrate. In the absence of TRX, TxR, PRX I or MST1 C, equal amounts of GST were added to adjust the total protein concentration. The kinase reaction was initiated by addition of 200 μM ATP or 1 μCi [γ -³²P]ATP and then incubated for 5 min at 30 °C. The reaction was then stopped by adding the SDS sample buffer. Samples were subjected to SDS-PAGE and immunoblotted with anti-p-CRMP2 antibody or the radioactivity of MOBKL1B was determined by autoradiography (BAS2000, FUJIFILM Corporation).

5.12. Apoptosis assay

U2OS cells were transfected with various expression plasmids or siRNAs together with GFP-expressing plasmids. Cells were cultured for 24 hours and then treated with 25 μM cisplatin for 48 hours. Cells were fixed with 3 % formaldehyde for 1 hour and stained with DAPI for 1 hour to visualize nuclei. Images were taken using an Olympus IX81 microscope equipped with an Olympus DP30BW camera. GFP-positive cells were assessed for their chromatin condensation. For each experiment, more than

100 cells were measured.

5.13. Real time PCR analyses

Real-time PCR experiments were performed with MiniOpticon (Bio-Rad) using the iQ SYBR green Supermix (Bio-Rad). The quality of the final PCR product was checked by agarose gel electrophoresis and it was confirmed that there were no obvious non-specifically amplified DNAs. The primers used are as follows: *PRX I* (5'-GACCCATGAACATTCCTTTG-3' and 5'-AGGCTTGATGGTATCACTGC-3'), *PRX II* (5'-GTCCGTGCGTCTAGCCTTTG-3' and 5'-TCCCTTTGTAGTCCGACAGC-3'), and *GAPDH* (5'-AGGTGAAGGTCCGAGTCAACG-3' and 5'-AGGGGTCATTGATGGCAACA-3').

5.14. Statistical analyses

All statistical analyses were done with the Student's t test. Error bars in the graphs represent standard error of the mean (SEM). Turning angle of growth cones, fluorescence intensities of GFP-HyPer and immunoblots were quantified by measuring scanned photographs in NIH Image J software (National Institutes of Health, U.S.A.).

6. References

1. T. Finkel, N. J. Holbrook, Oxidants, oxidative stress and the biology of ageing. *Nature* **408**, 239-247 (2000).
2. T. Finkel, Oxidant signals and oxidative stress. *Curr. Opin. Cell Biol.* **15**, 247-254 (2003).
3. S. G. Rhee, Cell signaling. H₂O₂, a necessary evil for cell signaling. *Science* **312**, 1882-1883 (2006).
4. B. D'Autreaux, M. B. Toledano, ROS as signalling molecules: mechanisms that generate specificity in ROS homeostasis. *Nat. Rev. Mol. Cell Biol.* **8**, 813-824 (2007).
64. E. A. Veal, A. M. Day, B. A. Morgan, Hydrogen peroxide sensing and signaling. *Mol. Cell* **26**, 1-14 (2007).
6. A. T. Saurin, H. Neubert, J. P. Brennan, P. Eaton, Widespread sulfenic acid formation in tissues in response to hydrogen peroxide. *Proc. Natl. Acad. Sci. U.S.A.* **101**, 17982-17987. (2004).
7. A. Holmgren, Thioredoxin structure and mechanism: conformational changes on oxidation of the active-site sulfhydryls to a disulfide. *Structure* **3**, 239-243 (1995).
8. C. H. Lillig, A. Holmgren, Thioredoxin and related molecules--from biology to health and disease. *Antioxid. Redox Signal.* **9**, 25-47 (2007).

9. R. Wynn, M. J. Cocco, F. M. Richards, Mixed disulfide intermediates during the reduction of disulfides by *Escherichia coli* thioredoxin. *Biochemistry* **34**, 11807-11813 (1995).
10. S. G. Rhee, H. Z. Chae, K. Kim, Peroxiredoxins: a historical overview and speculative preview of novel mechanisms and emerging concepts in cell signaling. *Free Radic. Biol. Med.* **38**, 1543-1552 (2005).
11. B. J. Dickson, Molecular mechanisms of axon guidance. *Science* **298**, 1959-1964 (2002).
12. J. A. Raper, Semaphorins and their receptors in vertebrates and invertebrates. *Curr. Opin. Neurobiol.* **10**, 88-94 (2000).
13. F. Nakamura, R. G. Kalb, S. M. Strittmatter, Molecular basis of semaphorin-mediated axon guidance. *J. Neurobiol.* **44**, 219-229 (2000).
14. U. Yazdani, J. R. Terman, The semaphorins. *Genome Biol.* **7**, 211-225 (2006).
15. Y. Goshima, F. Nakamura, P. Strittmatter, S. M. Strittmatter, Collapsin-induced growth cone collapse mediated by an intracellular protein related to UNC-33. *Nature* **376**, 509-514 (1995).
16. M. Brown, T. Jacobs, B. Eickholt, G. Ferrari, M. Teo, C. Monfries, R. Z. Qi, T. Leung, L. Lim, C. Hall, α 2-chimaerin, cyclin-dependent Kinase 5/p35, and its target collapsin response mediator protein-2 are essential components in semaphorin 3A-induced growth-cone collapse. *J. Neurosci.* **24**, 8994-9004 (2004).
17. Y. Uchida, T. Ohshima, Y. Sasaki, H. Suzuki, S. Yanai, N. Yamashita, F. Nakamura, K. Takei, Y. Ihara, K. Mikoshiba, P. Kolattukudy, J. Honnorat, Y. Goshima, Semaphorin3A signalling is mediated via sequential Cdk5 and GSK3 β

phosphorylation of CRMP2: implication of common phosphorylating mechanism underlying axon guidance and Alzheimer's disease. *Genes. Cells* **10**, 165-179 (2005).

- 18.** Y. Fukata, T. J. Itoh, T. Kimura, C. Menager, T. Nishimura, T. Shiromizu, H. Watanabe, N. Inagaki, A. Iwamatsu, H. Hotani, K. Kaibuchi, CRMP-2 binds to tubulin heterodimers to promote microtubule assembly. *Nat. Cell Biol.* **4**, 583-591 (2002).
- 19.** T. Yoshimura, Y. Kawano, N. Arimura, S. Kawabata, A. Kikuchi, K. Kaibuchi, GSK-3 β regulates phosphorylation of CRMP-2 and neuronal polarity. *Cell* **120**, 137-149 (2005).
- 20.** J. R. Terman, T. Mao, R. J. Pasterkamp, H. H. Yu, A. L. Kolodkin, MICALs, a family of conserved flavoprotein oxidoreductases, function in plexin-mediated axonal repulsion. *Cell* **109**, 887-900 (2002).
- 21.** E. F. Schmidt, S. O. Shim, S. M. Strittmatter, Release of MICAL autoinhibition by semaphorin-plexin signaling promotes interaction with collapsin response mediator protein. *J. Neurosci.* **28**, 2287-2297 (2008).
- 22.** M. Nadella, M. A. Bianchet, S. B. Gabelli, J. Barrila, L. M. Amzel, Structure and activity of the axon guidance protein MICAL. *Proc. Natl. Acad. Sci. U.S.A.* **102**, 16830-16835 (2005).
- 23.** R. J. Pasterkamp, H. N. Dai, J. R. Terman, K. J. Wahlin, B. Kim, B. S. Bregman, P. G. Popovich, A. L. Kolodkin, MICAL flavoprotein monooxygenases: expression during neural development and following spinal cord injuries in the rat. *Mol. Cell. Neurosci.* **31**, 52-69 (2006).

24. R. J. Hung, U. Yazdani, J. Yoon, H. Wu, T. Yang, N. Gupta, Z. Huang, W. J. van Berkel, J. R. Terman, Mical links semaphorins to F-actin disassembly. *Nature* **463**, 823-827 (2010).
25. Y. Funato, H. Miki, Nucleoredoxin, a novel thioredoxin family member involved in cell growth and differentiation. *Antioxid. Redox Signal.* **9**, 1035-1057 (2007).
26. N. Inagaki, K. Chihara, N. Arimura, C. Menager, Y. Kawano, N. Matsuo, T. Nishimura, M. Amano, K. Kaibuchi, CRMP-2 induces axons in cultured hippocampal neurons. *Nat. Neurosci.* **4**, 781-782. (2001)
27. H. Kurooka, K. Kato, S. Minoguchi, Y. Takahashi, J. Ikeda, S. Habu, N. Osawa, A. M. Buchberg, K. Moriwaki, H. Shisa, T. Honjo, Cloning and characterization of the nucleoredoxin gene that encodes a novel nuclear protein related to thioredoxin. *Genomics* **39**, 331-339 (1997).
28. K. K. Lee, M. Murakawa, S. Takahashi, S. Tsubuki, S. Kawashima, K. Sakamaki, S. Yonehara, Purification, molecular cloning, and characterization of TRP32, a novel thioredoxin-related mammalian protein of 32 kDa. *J. Biol. Chem.* **273**, 19160-19166 (1998).
29. W. Jeong, H. W. Yoon, S. R. Lee, S. G. Rhee, Identification and characterization of TRP14, a thioredoxin-related protein of 14 kDa. New insights into the specificity of thioredoxin function. *J. Biol. Chem.* **279**, 3142-3150 (2004).
30. Y. Tada, S. H. Spoel, K. Pajerowska-Mukhtar, Z. Mou, J. Song, C. Wang, J. Zuo, X. Dong, Plant immunity requires conformational changes of NPR1 via S-nitrosylation and thioredoxins. *Science* **321**, 952-956 (2008).

- 31.** S. R. Jaffrey, H. Erdjument-Bromage, C. D. Ferris, P. Tempst, S. H. Snyder, Protein S-nitrosylation: a physiological signal for neuronal nitric oxide. *Nat. Cell Biol.* **3**, 193-197 (2001).
- 32.** G. Hao, B. Derakhshan, L. Shi, F. Campagne, S. S. Gross, SNOSID, a proteomic method for identification of cysteine S-nitrosylation sites in complex protein mixtures. *Proc. Natl. Acad. Sci. U.S.A.* **103**, 1012-1017 (2006).
- 33.** J. Oblong, M. Berggren, P. Y. Gasdaska, G. Powin, Site-directed mutagenesis of active site cysteines in human thioredoxin produces competitive inhibitors of human thioredoxin reductase and elimination of mitogenic properties of thioredoxin. *J. Biol. Chem.* **269**, 11714-11720 (1994).
- 34.** T. Tojima, R. Itofusa, H. Kamiguchi, Asymmetric clathrin-mediated endocytosis drives repulsive growth cone guidance. *Neuron* **66**, 370-377 (2010).
- 35.** E. S. Arner, M. Bjornstedt, A. Holmgren, 1-Chloro-2,4-dinitrobenzene is an irreversible inhibitor of human thioredoxin reductase. Loss of thioredoxin disulfide reductase activity is accompanied by a large increase in NADPH oxidase activity. *J. Biol. Chem.* **270**, 3479-3482 (1995).
- 36.** G. Chen, J. Sima, M. Jin, K. Y. Wang, X. J. Xue, W. Zheng, Y. Q. Ding, X. B. Yuan, Semaphorin-3A guides radial migration of cortical neurons during development. *Nat. Neurosci.* **11**, 36-44 (2007).
- 37.** V. V. Belousov, A. F. Fradkov, K. A. Lukyanov, D. B. Staroverov, K. S. Shakhbazov, A. V. Terskikh, S. Lukyanov, Genetically encoded fluorescent indicator for intracellular hydrogen peroxide. *Nat. Methods* **3**, 281-286 (2006).

- 38.** T. Nishimura, Y. Fukata, K. Kato, T. Yamaguchi, Y. Matsuura, H. Kamiguchi, K. Kaibuchi, CRMP-2 regulates polarized Numb-mediated endocytosis for axon growth. *Nat. Cell Biol.* **5**, 819-26 (2003).
- 39.** T. Kimura, H. Watanabe, A. Iwamatsu, K. Kaibuchi, Tubulin and CRMP-2 complex is transported via Kinesin-1. *J. Neurochem.* **93**, 1371-1382 (2005).
- 40.** Y. Kawano, T. Yoshimura, D. Tsuboi, S. Kawabata, T. Kaneko-Kawano, H. Shirataki, T. Takenawa, K. Kaibuchi, CRMP-2 is involved in kinesin-1-dependent transport of the Sra-1/WAVE1 complex and axon formation. *Mol. Cell Biol.* **25**, 9920-9935 (2005).
- 41.** N. Arimura, T. Kimura, S. Nakamuta, S. Taya, Y. Funahashi, A. Hattori, A. Shimada, C. Menager, S. Kawabata, K. Fujii, A. Iwamatsu, R. A. Segal, M. Fukuda, K. Kaibuchi, Anterograde transport of TrkB in axons is mediated by direct interaction with Slp1 and Rab27. *Dev. Cell* **16**, 675-686 (2009).
- 42.** N. Arimura, A. Hattori, T. Kimura, S. Nakamuta, Y. Funahashi, S. Hirotsune, K. Furuta, T. Urano, Y. Y. Toyoshima, K. Kaibuchi, CRMP-2 directly binds to cytoplasmic dynein and interferes with its activity. *J. Neurochem.* **111**, 380-390 (2009).
- 43.** N. Arimura, C. Menager, Y. Kawano, T. Yoshimura, S. Kawabata, A. Hattori, Y. Fukata, M. Amano, Y. Goshima, M. Inagaki, N. Morone, J. Usukura, K. Kaibuchi, Phosphorylation by Rho kinase regulates CRMP-2 activity in growth cones. *Mol. Cell. Biol.* **25**, 9973-9984 (2005).
- 44.** Y. Sasaki, C. Cheng, Y. Uchida, O. Nakajima, T. Ohshima, T. Yagi, M. Taniguchi, T. Nakayama, R. Kishida, Y. Kudo, S. Ohno, F. Nakamura Y. Goshima Y, Fyn and

Cdk5 mediate semaphorin-3A signaling, which is involved in regulation of dendrite orientation in cerebral cortex. *Neuron* **35**, 907-920 (2002).

- 45.** I. Oinuma, Y. Ishikawa, H. Katoh, M. Negishi, The Semaphorin 4D receptor Plexin-B1 is a GTPase activating protein for R-Ras. *Science* **305**, 862-865 (2004).
- 46.** Y. Ito, I. Oinuma, H. Katoh, K. Kaibuchi, M. Negishi, Sema4D/plexin-B1 activates GSK-3 β through R-Ras GAP activity, inducing growth cone collapse. *EMBO Rep.* **7**, 704-709 (2006).
- 47.** J. K. Suh, L. L. Poulsen, D. M. Ziegler, J. D. Robertus, Molecular cloning and kinetic characterization of a flavin-containing monooxygenase from *Saccharomyces cerevisiae*. *Arch. Biochem. Biophys.* **336**, 268-74 (1996).
- 48.** S. K. Krueger, D. E. Williams, Mammalian flavin-containing monooxygenases: structure/function, genetic polymorphisms and role in drug metabolism. *Pharmacol. Ther.* **106**, 357-387 (2005).
- 49.** C. Siebold, N. Berrow, T. S. Walter, K. Harlos, R. J. Owens, D. I. Stuart, J. R. Terman, A. L. Kolodkin, R. J. Pasterkamp, E. Y. Jones, High-resolution structure of the catalytic region of MICAL (molecule interacting with CasL), a multidomain flavoenzyme-signaling molecule. *Proc. Natl. Acad. Sci. U.S.A.* **102**, 16836-16841 (2005).
- 50.** R. C. Deo, E. F. Schmidt, A. Elhabazi, H. Togashi, S. K. Burley, S. M. Strittmatter, Structural bases for CRMP function in plexin-dependent semaphorin3A signaling. *EMBO J.* **23**, 9-22 (2004).

51. P. Stenmark, D. Ogg, S. Flodin, A. Flores, T. Kotenyova, T. Nyman, P. Nordlund, P. Kursula, The structure of human collapsin response mediator protein 2, a regulator of axonal growth. *J. Neurochem.* **101**, 906-917 (2007).
52. L. H. Wang, S. M. Strittmatter, Brain CRMP forms heterotetramers similar to liver dihydropyrimidinase. *J. Neurochem.* **69**, 2261-2269 (1997).
53. M. Karin, T. Hunter, Transcriptional control by protein phosphorylation: signal transmission from the cell surface to the nucleus. *Curr. Biol.* **5**, 747-757 (1995).
54. P. M. de Souza, M. A. Lindsay, Mammalian Sterile20-like kinase 1 and the regulation of apoptosis. *Biochem. Soc. Trans.* **32**, 485-488 (2004).
55. M. K. Lehtinen, Z. Yuan, P. R. Boag, Y. Yang, J. Villen, E. B. Becker, S. DiBacco, N. de la Iglesia, S. Gygi, T. K. Blackwell, A. Bonni, A conserved MST-FOXO signaling pathway mediates oxidative-stress responses and extends life span. *Cell* **125**, 987-1001 (2006).
56. S. H. Ahn, W. L. Cheung, J. Y. Hsu, R. Z. Diaz, M. M. Smith, C. D. Allis, Sterile 20 kinase phosphorylates histone H2B at serine 10 during hydrogen peroxide-induced apoptosis in *S. cerevisiae*. *Cell* **120**, 25-36 (2005).
57. E. E. O'Neill, D. Matallanas, W. Kolch, Mammalian sterile 20-like kinases in tumor suppression: an emerging pathway. *Cancer Res.* **65**, 5485-5487 (2005).
58. A. Ren, G. Yan, B. You, J. Sun, Down-regulation of mammalian sterile 20-like kinase 1 by heat shock protein 70 mediates cisplatin resistance in prostate cancer cells. *Cancer Res.* **68**, 2266-2274 (2008).
59. S. W. Lowe, H. E. Ruley, T. Jacks, D. E. Housman, p53-dependent apoptosis modulates the cytotoxicity of anticancer agents. *Cell* **74**, 957-967 (1993).

- 60.** S. W. Lowe, S. Bodis, A. McClatchey, L. Remington, H. E. Ruley, D. E. Fisher, D. E. Housman, T. Jacks, p53 status and the efficacy of cancer therapy *in vivo*. *Science* **266**, 807-810 (1994).
- 61.** J. Colombani, C. Polesello, F. Josué, N. Tapon, Dmp53 activates the Hippo pathway to promote cell death in response to DNA damage. *Curr. Biol.* **16**, 1453-1458 (2006).
- 62.** T. M. Johnson, Z. X. Yu, V. J. Ferrans, R. A. Lowenstein, T. Finkel, Reactive oxygen species are downstream mediators of p53-dependent apoptosis. *Proc. Natl. Acad. Sci. U.S.A.* **93**, 11848-11852 (1996).
- 63.** K. Polyak, Y. Xia, J. L. Zweier, K. W. Kinzler, B. Vogelstein, A model for p53-induced apoptosis. *Nature* **389**, 300-305 (1997).
- 64.** P. F. Li, R. Dietz, R. von Harsdorf, p53 regulates mitochondrial membrane potential through reactive oxygen species and induces cytochrome c-independent apoptosis blocked by Bcl-2. *EMBO J.* **18**, 6027-6036 (1999).
- 65.** H. H. Jang, K. O. Lee, Y. H. Chi, B. G. Jung, S. K. Park, J. H. Park, J. R. Lee, S. S. Lee, J. C. Moon, J. W. Yun, Y. O. Choi, W. Y. Kim, J. S. Kang, G. W. Cheong, D. J. Yun, S. G. Rhee, M. J. Cho, S. Y. Lee, Two enzymes in one; two yeast peroxiredoxins display oxidative stress-dependent switching from a peroxidase to a molecular chaperone function. *Cell* **117**, 625-635 (2004).
- 66.** E. A. Veal, V. J. Findlay, A. M. Day, S. M. Bozonet, J. M. Evans, J. Quinn, B. A. Morgan, A 2-Cys peroxiredoxin regulates peroxide-induced oxidation and activation of a stress-activated MAP kinase. *Mol. Cell* **15**, 129-139 (2004).
- 67.** W. Lee, K. S. Choi, J. Riddell, C. Ip, D. Ghosh, J. H. Park, Y. M. Park, Human peroxiredoxin 1 and 2 are not duplicate proteins: the unique presence of CYS83 in

- Prx1 underscores the structural and functional differences between Prx1 and Prx2. *J. Biol. Chem.* **282**, 22011-22022 (2007).
- 68.** M. Praskova, A. Khoklatchev, S. Ortiz-Vega, J. Avruch. Regulation of the MST1 kinase by autophosphorylation, by the growth inhibitory proteins, RASSF1 and NORE1, and by Ras. *Biochem. J.* **381**, 453-462 (2004).
- 69.** K. Z. Guyton, Y. Liu, M. Gorospe, Q. Xu, H. J. Holbrook, Activation of mitogen-activated protein kinase by H₂O₂. Role in cell survival following oxidant injury. *J. Biol. Chem.* **271**, 4138-4142 (1996).
- 70.** M. Praskova, F. Xia, J. Avruch, MOBKL1A/MOBKL1B phosphorylation by MST1 and MST2 inhibits cell proliferation. *Curr. Biol.* **18**, 311-321 (2008).
- 71.** P. Perego, S. C. Righetti, R. Supino, D. Delia, C. Caserini, N. Carenini, B. Bedogne, E. Broome, S. Krajewski, J. C. Reed, F. Zunino, Role of apoptosis and apoptosis-related proteins in the cisplatin-resistant phenotype of human tumor cell lines. *Apoptosis* **2**, 540-548 (1997).
- 72.** C. L. Creasy, D. M. Ambrose, J. Chernoff, The Ste20-like protein kinase, Mst1, dimerizes and contains an inhibitory domain. *J. Biol. Chem.* **271**, 21049-21053 (1996).
- 73.** D. Trachootham, J. Alexandre, P. Huang P, Targeting cancer cells by ROS-mediated mechanisms: a radical therapeutic approach? *Nat. Rev. Drug Discov.* **8**, 579-591 (2009).
- 74.** D. Trachootham, Y. Zhou, H. Zhang, Y. Demizu, Z. Chen, H. Pelicano, P. J. Chiao, G. Achanta, R. B. Arlinghaus, J. Liu, P. Huang, Selective killing of oncogenically transformed cells through a ROS-mediated mechanism by β -phenylethyl isothiocyanate. *Cancer Cell* **10**, 241-252 (2006).

- 75.** K. Harvey, N. Tapon, The Salvador-Warts-Hippo pathway - an emerging tumour-suppressor network. *Nat. Rev. Cancer* **7**, 182-191 (2007).
- 76.** Q. Zeng, W. Hong, The emerging role of the hippo pathway in cell contact inhibition, organ size control, and cancer development in mammals. *Cancer Cell* **13**, 188-192 (2008).
- 77.** C. A. Neumann, D. S. Krause, C. V. Carman, S. Das, D. P. Dubey, J. L. Abraham, R. T. Bronson, Y. Fujiwara, S. H. Orkin, R. A. Van Etten, Essential role for the peroxiredoxin Prdx1 in erythrocyte antioxidant defence and tumour suppression. *Nature* **424**, 561-565 (2003).
- 78.** R. A. Egler, E. Fernandes, K. Rothermund, S. Sereika, N. de Souza-Pinto, P. Jaruga, M. Dizdaroglu, E. V. Prochownik, Regulation of reactive oxygen species, DNA damage, and c-Myc function by peroxiredoxin 1. *Oncogene* **24**, 8038-8050 (2005).
- 79.** J. A. Graves, M. Metukuri, D. Scott, K. Rothermund, E. V. Prochownik, Regulation of reactive oxygen species homeostasis by peroxiredoxins and c-Myc. *J. Biol. Chem.* **284**, 6520-6529 (2009).
- 80.** M. H. Choi, I. K. Lee, G. W. Kim, B. U. Kim, Y. H. Han, D. Y. Yu, H. S. Park, K. Y. Kim, J. S. Lee, C. Choi, Y. S. Bae, B. I. Lee, S. G. Rhee, S. W. Kang, Regulation of PDGF signalling and vascular remodelling by peroxiredoxin II. *Nature* **435**, 347-353 (2005).
- 81.** J. C. Moon, Y. S. Hah, W. Y. Kim, B. G. Jung, H. H. Jang, J. R. Lee, S. Y. Kim, Y. M. Lee, M. G. Jeon, G. W. Kim, M. J. Cho, S. Y. Lee, Oxidative stress-dependent structural and functional switching of a human 2-Cys peroxiredoxin isotype II that enhances HeLa cell resistance to H₂O₂-induced cell

- death. *J. Biol. Chem.* **280**, 28775-28784 (2005).
- 82.** K. Takenaka, Y. Kise, H. Miki, GSK3 β positively regulates Hedgehog signaling through Sufu in mammalian cells. *Biochem. Biophys. Res. Commun.* **353**, 501-508 (2007).
- 83.** Y. Funato, T. Michiue, M. Asashima, H. Miki, The thioredoxin-related redox-regulating protein nucleoredoxin inhibits Wnt- β -catenin signalling through dishevelled. *Nat. Cell Biol.* **8**, 501-508 (2006).
- 84.** T. Tsukada, Y. Tomooka, S. Takai, Y. Ueda, S. Nishikawa, T. Yagi, T. Tokunaga, N. Takeda, Y. Suda, S. Abe, *et al.*, Enhanced proliferative potential in culture of cells from p53-deficient mice. *Oncogene* **8**, 3313-3322 (1993).
- 85.** T. Iwamura, M. Yoneyama, K. Yamaguchi, W. Suhara, W. Mori, K. Shiota, Y. Okabe, H. Namiki, T. Fujita, Induction of IRF-3/-7 kinase and NF- κ B in response to double-stranded RNA and virus infection: common and unique pathways. *Genes Cells* **6**, 375-388 (2001).
- 86.** H. Akiyama, T. Matsu-ura, K. Mikoshiba, H. Kamiguchi, Control of neuronal growth cone navigation by asymmetric inositol 1,4,5-trisphosphate signals. *Sci. Signal.* **2**, ra34 (2009).
- 87.** T. Kawauchi, K. Chihama, Y. Nabeshima, M. Hoshino, The *in vivo* roles of STEF/Tiam1, Rac1 and JNK in cortical neuronal migration. *EMBO J.* **22**, 4190-4201 (2003).
- 88.** T. Kawauchi, K. Chihama, Y. Nabeshima, M. Hoshino, Cdk5 phosphorylates and stabilizes p27kip1, contributing to actin organization and cortical neuronal migration. *Nat. Cell Biol.* **8**, 17-26 (2006).

7. Acknowledgements

I would like to acknowledge Dr. Mayumi Yamada and Dr. Mikio Hoshino (National Institute of Neuroscience) for performing *in utero* electroporation, Dr. Rurika Itofusa, Dr. Hiroyuki Kamiguchi (RIKEN Brain Science Institute), Dr. Fumio Nakamura and Dr. Yoshio Goshima (Yokohama City University) for training me in experiments using DRG neurons and Dr. Takeshi Yoshimura and Dr. Kozo Kaibuchi (Nagoya University) for generating anti-p-CRMP2 antibody. I would also like to acknowledge Dr. Yosuke Funato, Dr. Yuta Yoshimura, Dr. Kanami Uesugi (Osaka University) and Dr. Yoshiaki Kise (Flanders Institute for Biotechnology, Belgium) for technical assistance and helpful discussion. I thank Dr. Shinobu Ohmi (University of Tokyo) and Dr. Hiroyuki Fukuda (THERAVALUES Corporation) for technical help with mass spectrometry.

I am grateful to Dr. Sumio Sugano (Tokyo University) and Dr. Hiroaki Miki (Osaka University) for educating me in all respects of this research as graduate advisors and all members of my laboratory for supporting me both officially and privately.

Finally, I wish sincerely to express our gratitude to my parents for affectionate support for years.